ATMOSPHERIC TRANSPORT OF HYDROGEN SULFIDE FROM PROPOSED GEOTHERMAL POWER PLANT (UNIT 16)

Predictions by Physical Modeling
in a Wind Tunnel

by

J. E. Cermak* and R. L. Petersen**

Prepared for

Pacific Gas and Electric Company
San Francisco, California

Fluid Dynamics and Diffusion Laboratory
Fluid Mechanics and Wind Engineering Program
Colorado State University
Fort Collins, Colorado
80523

March 1977

CER76-77JEC-RLP4

*Director, Fluid Dynamics and Diffusion Laboratory
**Graduate Research Assistant, Department of Civil Engineering

ABSTRACT

Tests were conducted in the Colorado State University environmental wind tunnel facility of the transport and dispersion of the H_2S plume emanating from a cooling tower positioned at two locations near Anderson Springs, California. The wind tunnel tests were conducted with a cooling tower and terrain modeled to a scale of 1:1920. The effects of wind direction and wind speed upon the ground-level H_2S concentrations in the vicinity of Anderson Springs were established. Data obtained include photographs and motion pictures of smoke plume trajectories and ground-level tracer gas concentrations downwind of the cooling tower.

ACKNOWLEDGMENTS

Mr. James A. Garrison supervised construction of the terrain model and photographic recording of the flow visualizations. Mr. Samir Ayad collected and processed all hot-wire and smoke-wire velocity data. The authors also acknowledge the assistance of Mrs. Stephanie Allen in typing and organizing this report. The help of the following students throughout the research is appreciated: Messrs. Stan Schwartz, David Graham, Tom Zook, Jim DeCino, Chris Leveroni, John Elmer, and Herb Riehl.

TABLE OF CONTENTS

LIST OF FIGURES

LIST OF FIGURES
(continued)

LIST OF FIGURES
(continued)

LIST OF FIGURES
(continued)

LIST OF TABLES

LIST OF SYMBOLS

Symbol	Definition	Dimensions
D	Stack Diameter	(L)
E	Gas Chromatograph Response	(mvs)
Fr	Froude number $\frac{V^2}{g(\frac{\Delta\rho}{\rho_a})\ D}$	(-)
g	Gravitational Constant	(L/T^2)
h	Cooling Tower Height	(L)
H	Height of Terrain Above Cooling Tower Elevation	
k	von Karman Constant	(-)
K	Concentration Isopleth	(-)
L_o	Distance from Beginning of Wind Tunnel	(L)
Q_s	Source Strength	(M/T)
R	Exhaust Velocity Ratio V_s/V_a	(-)
Re_{L_o}	Reynolds number $\frac{VL_o}{\nu}$	(-)
U_*	Friction Velocity	(L/T)
V	Mean Velocity	(L/T)
x,y	General Coordinates -- downwind, lateral	(L)
z_o	Surface Roughness Parameter	(L)

LIST OF SYMBOLS
(continued)

Symbol	Definition	Dimensions
(Greek Symbols)		
χ	Local Concentration	(M/L^3 or ppm)
τ	Sampling Time	(T)
θ	Azimuth Angle of Upwind Direction Measured From Plant North	(-)
σ	Standard Deviation of Either Plume Dispersion or Wind Angle Fluctuations	(L) (-)
ν	Kinematic Viscosity	(L^2/T)
δ	Boundary Layer Thickness	(L)
γ	Specific Weight	$M(T^2L^2)$
ρ	Density	(M/L^3)
Ω	Angular Velocity	(1/T)
μ	Dynamic Viscosity	M/(TL)
Λ	Volume Flow Rate	(L^3/T)
Subscripts		
a	Meteorological Tower	
s	Stack	
m	Model	
p	Prototype	
max	Maximum	
g	Geostrophic or Gradient Wind	
rms	Root Mean Square	
∞	Reference Value	

CONVERSION TABLE

(English to Metric Units)

Multiply Units	by	To Obtain
inches	2.540	centimeters
square inches	6.452	square centimeters
cubic inches	16.39	cubic centimeters
feet	0.3048	meters
square feet	0.0929	square meters
cubic feet	0.02832	cubic meters
feet/second	0.3048	meters/second
miles/hour	0.4470	meters/second
cubic feet/minute	0.02832	cubic meters/minute
cubic feet/minute	0.00047	cubic meters/second

1.0 INTRODUCTION

The purpose of this study was to determine the transport characteristics of hydrogen sulfide released in plumes emanating from the cooling tower of a proposed new geothermal power plant (Unit 16) in the Geysers Geothermal Area. Using a 1:1920 scale model of the cooling tower and surrounding topography in a wind tunnel capable of simulating the appropriate meteorological conditions, two possible locations for the power plant were studied. These locations are shown in Figure 1.1 in relation to Anderson Springs and Whispering Pines.

Downwind ground-level H_2S concentrations were determined by sampling concentrations of a tracer gas (propane) released from the model cooling tower. Overall plume geometry was obtained by photographing the plumes made visible by releasing smoke (titanium tetrachloride) from the model cooling tower.

The primary focus of this study was on the H_2S concentrations in the vicinity of Anderson Springs for neutral thermal stratification. Accordingly, studies of the upper-level winds were confined to three directions: 210°, 230°, and 250° azimuth. Figure 1.2 shows the wind rose which was obtained from a meteorological tower (Site 6) in the vicinity of Units 7 and 8 which is considered representative of ridge-line flow. Information from the meteorological station indicated that winds in the sector 210° to 250° occur approximately 40 per cent of the time. Wind speeds of 3.2, 6.5, and 9.8 m/s at the meteorological station were modeled to obtain representative concentrations under beneficial and adverse plume rise conditions.

Another objective was to relate wind speed at the proposed Unit 16 sites to that at the meteorological station in the area and the upper-level (ambient) wind speed in the wind tunnel.

Included in this report are a brief description of the similarity requirements for atmospheric motion, an explanation of test methodology and procedures, results of plume visualization and concentration measurements, and results of wind flow measurements.

This report is supplemented by a motion picture (in color) which shows plume behavior for the various wind speed and wind direction test scenarios. Black and white photographs as well as slides of each plume visualization further illustrate the material presented.

2.0 SIMULATION OF ATMOSPHERIC MOTION

The use of wind tunnels for model tests of gas diffusion by the atmosphere is based upon the concept that nondimensional concentration coefficients will be the same at corresponding points in the model and the prototype and will not be a function of the length scale ratio. Concentration coefficients will only be independent of scale if the wind tunnel boundary layer is made similar to the atmospheric boundary layer by satisfying certain similarity criteria. These criteria are obtained by inspectional analysis of physical statements for conservation of mass, momentum, and energy. Detailed discussions have been given by Halitsky (1963), Martin (1965), and Cermak, et al. (1966). Basically, the model laws may be divided into requirements for geometric, dynamic, thermic, and kinematic similarity. In addition, similarity of upwind flow characteristics and ground boundary conditions must be achieved.

For this study, geometric similarity is satisfied by an undistorted model of length ratio 1:1920. This scale was chosen to facilitate ease of measurements and to provide a representative upwind fetch.

When interest is focused on the vertical motion of plumes of heated gases emitted from stacks into a thermally neutral atmosphere, the following variables are of primary significance:

ρ_a = density of ambient air

$\Delta\gamma$ = $(\rho_a - \rho_s)g$ -- difference in specific weight of ambient air and cooling tower gas

Ω = local angular velocity component of earth

μ_a = dynamic viscosity of ambient air

V_a = speed of ambient wind at meteorological tower

V_s = speed of tower gas emission

h = cooling tower height

H = local difference in elevation of topograph

D = cooling tower diameter

δ_a = thickness of planetary boundary layer

z_o = roughness heights for upwind surface

Grouping the independent variables into dimensionless parameters with ρ_a, V_a and H as reference variables yields the following parameters upon which the dependent quantities of interest must depend:

$$\frac{V_a}{H\Omega}, \frac{\delta_a}{H}, \frac{z_o}{H}, \frac{D}{H}, \frac{V_a \rho_a H}{\mu_a}, \frac{V_s}{V_a}, \frac{\rho_a V_a^2}{\Delta\gamma D}, \frac{\Delta\gamma}{g\rho}$$

Tables 2.1 and 2.2 summarize the pertinent dimensional and dimensionless parameters relevant to this study.

The laboratory boundary-layer thickness $\frac{\delta_a}{H}$ was estimated to be nearly equal for model and prototype. Near equality (within a factor of two) of the surface parameter $\frac{z_o}{H}$ for model and prototype was achieved through geometrical scaling of the cooling towers and upwind roughness. The cooling tower parameter $\frac{D}{H}$ was equal for model and prototype.

The magnitude of the roughness parameter, z_o, for the model was calculated by using the logarithmic wind equation

$$\frac{V}{U_*} = \frac{1}{k} \ell n \left(\frac{z}{z_o}\right)$$

The wind speeds at heights 0.97 cm and 2.24 cm above the location of the meteorological tower in the model were substituted into the equation. With the resulting two equations, z_o (and U_*) was calculated. The magnitude of z_o for the prototype was estimated by reference to a plot of z_o versus terrain type presented in Cermak (1975).

Dynamic similarity is achieved in a strict sense if the Reynolds number, $\frac{\rho_a V_a L_o}{\mu_a}$, and Rossby number, $\frac{V_a}{H\Omega}$, for the model are equal to their counterparts in the atmosphere. The model Rossby number cannot be made equal to the atmospheric value. However, over the short distances considered (up to 5000 m), the Coriolis acceleration has little influence upon the flow. Accordingly, the standard practice is to relax the requirement of equal Rossby numbers (Cermak, 1971).

Kinematic similarity requires the scaled equivalence of streamline movement of the air over prototype and model. It has been shown in Halitsky et al. (1963) that flow around geometrically similar sharp-edged buildings at ambient temperatures in a neutrally stratified atmosphere should be dynamically and kinematically similar. This approach depends upon producing flows in which the flow characteristics become independent of Reynolds number if a lower limit of

the Reynolds number is exceeded. For example, the resistance coefficient for flow in a sufficiently rough pipe, as shown in Schlichting (1960), p. 521), is constant for a Reynolds number larger than 2×10^4. This implies that surface or drag forces are directly proportional to the mean flow speed squared. In turn, this condition is the necessary condition for mean turbulence statistics such as root-mean square value and correlation coefficient of the turbulence velocity components to be equal for the model and the prototype flow.

Equality of the parameter $\frac{\rho_a V_a^2}{\Delta\gamma D}$ for model and prototype in essence determines the relationship between the atmospheric wind speed and the model wind speed once the geometric scale has been selected (1:1920 in this case). Often this criteria results in $(V_a)_m$ being too small to satisfy the minimum Reynolds number requirement. When this happens, the specific weight difference for the model $(\Delta\gamma)_m$ can be made larger than $(\Delta\gamma)_p$ to compensate for the effect of small geometric scale. However, this relaxes the equality of the density difference ratio for model and prototype. This equality ensures that the initial plume behavior where acceleration of the tower gases is maximum will be modeled correctly. However, since the measured concentrations for this study are not in the building vicinity, relation of this requirement is justified. More important is attainment of equal Froude numbers and equal values of the velocity ratio V_s/V_a for model and prototype.

Using a wind speed of $(V_a)_p$ of 3.2 m/s, a scale of 1:1920, and a specific weight ratio $\frac{(\Delta\gamma)_m}{(\Delta\gamma)_p} = 7.2$, the Froude number equality gives

$$\frac{(V_a)^2_m}{(V_a)^2_p} = \frac{1}{1920} \frac{(\Delta\gamma)_m}{(\Delta\gamma)_p} \qquad \text{or}$$

$$(V_a)_m = (\frac{1}{43.8}) \quad (7.2) \quad (3.2) = 0.20 \text{ m/s} .$$

The corresponding representative model velocity at a height of 0.46 m (878 m prototype) is 0.34 m/s. Using this velocity as the freestream velocity and a distance of 13.6 m from the beginning of the wind tunnel to the test site, the Reynolds number becomes

$$Re_{L_o} = \frac{0.34 \text{ X } 13.6}{15 \text{ X } 10^{-6}} = 3.1 \text{ X } 10^5 .$$

Referring to Figure 2.1 from Cermak (1975) it can be seen that for a Reynolds number of $3.1 \text{ X } 10^5$ the ratio of surface length to roughness length L_o/K_s must be less than 250 for the flow to be independent of Reynolds number. Thus K_s, the roughness length, must be greater than $\frac{13.6}{250}$ or 0.054 m. Taking the ridge height as the roughness height, K_s, results in $K_s = 0.10$ m, which is greater than the critical value of 0.054. Consequently, the flow over the test section is Reynolds number independent.

The method used to increase the Reynolds number such that the flow was independent of Re was to increase the specific weight difference between model and prototype. Since $\frac{(\Delta\gamma)_m}{(\Delta\gamma)_p} = 7.2$ represented the maximum specific weight difference practically attainable, the greatest increase in the local Reynolds number was achieved using this difference. Since the minimum Reynolds number for the cases studied was 3.1×10^5, similarity of concentration distributions over the topographic surface can be assured for all wind speeds studied.

To summarize, the following scaling criteria were applied for the neutral boundary layer situation:

1. $Fr = \frac{\rho_a V_a^2}{\Delta\delta D}$; $(Fr)_m = (Fr)_p$,

2. $R = \frac{V_s}{V_a}$; $R_m = R_p$,

3. $L_o/K_s > 250$ (implies Reynolds number independence),

4. $(z_o)_m = (z_o)_p$,

5. Similar geometric dimensions, and

6. Similar velocity and turbulence profiles upwind.

3.0 TEST APPARATUS

3.1 Wind Tunnels

The environmental wind tunnel (EWT) shown in Figure 3.1 was used for this neutral flow study. This wind tunnel, especially designed to study atmospheric flow phenomena, incorporates special features such as adjustable ceiling, rotating turntables, transparent boundary walls, and a long test section to permit adequate reproduction of micro-meteorological behavior. Mean wind speeds of 0.06 to 37 m/s (.14 to 80 miles/hour) in the EWT can be obtained. In the EWT, boundary layers four feet thick over the downstream 12.2 meters can be obtained with the use of vortex generators at the test section entrance. The flexible test section roof on the EWT is adjustable in height to permit the longitudinal pressure gradient to be set at zero.

3.2 Model

The model cooling tower was modeled at a scale of 1:1920. The relevant building dimensions are given in Table 2.1 and a photograph of the model is shown in Figure 3.2-1.

Topography was modeled to the same scale by cutting styrofoam sheets of 0.6 cm and 1.27 cm thicknesses to match contour lines of a topographic map enlarged to the 1:1920 scale. The topography for the 210° wind direction is shown mounted in the wind tunnel in Figure 3.2-2. The model terrain was not smoothed so as to increase the surface roughness and thereby prevent the formation of a laminar sublayer. This increased roughness also contributed toward achieving Reynolds number independence of flow over the test section.

Sections of modeled topography for the three wind directions were constructed for regions upwind and downwind of the topography mounted on the 3.66 m diameter turntable. In this way, rectangular regions could be fitted into the wind-tunnel test section.

An array of sampling tubes was inserted into the model terrain to give a minimum of 34 representative sampling locations for each wind direction. The sampling locations for each wind direction are shown in Figure 4.2-10, 4.2-11, and 4.2-12 and enumerated in Table 4.2-4.

Metered quantities of gas were allowed to flow from the cooling tower to simulate the exit velocity. Helium, compressed air, and propane (the tracer) were mixed to give the highest practical specific weight. Fischer-Porter flow meter settings were adjusted for pressure, temperature, and molecular weight effects as necessary. When a visible plume was required, the gas was bubbled through titanium tetrachloride before emission.

3.3 Flow Visualization Techniques

Smoke was used to define plume behavior from the geothermal power plant complex. The smoke was produced by passing the air mixture through a container of titanium tetrachloride located outside the wind tunnel and transported through the tunnel wall by means of a tygon tube terminating at the cooling-tower inlet. A schematic of the process is shown in Figure 3.3-1.

The plume was illuminated with arc-lamp beams and a visible record was obtained by means of pictures taken with a Speed Graphic camera. Additional still pictures were obtained with a Hasselblad

camera. Stills were taken with a camera speed of one second to identify mean plume boundaries. A series of 16 mm color motion pictures was also taken with a Bolex motion-picture camera.

3.4 Gas Tracer Technique

After the desired tunnel speed was obtained, a mixture of propane, helium, and air of predetermined concentration was released from the cooling tower at the required rate to simulate prototype plume rise. Samples of air were withdrawn from the sample points and analyzed. The flow rate of propane mixture was controlled by a pressure regulator at the supply cylinder outlet and monitored by a Fischer-Porter precision flow meter. The sampling system is shown in Figure 3.4-1.

-Analysis of Data-

Propane is an excellent tracer gas in wind-tunnel dispersion studies. It is a gas that is readily obtainable and of which concentration measurements are easily obtained using gas chromatography techniques.

The procedure for analyzing the samples was as follows:

1. A sample volume drawn from the wind tunnel of 2 cc was introduced into the Flame Ionization Detector.
2. The output from the electrometer (in millivolt seconds) was integrated and then the readings were recorded for each sample.
3. These readings were transformed into propane concentration values by the following steps:

$$\chi(\text{ppm}) = C(\text{ppm/mvs})E(\text{mvs})$$

where C was determined from a calibration gas of known concentration

$$C = (\text{ppm/mvs})_{\text{calibration gas}}.$$

The values of the concentration parameter initially determined apply to the model and it is desirable to express these values in terms of the field. At the present time, there is no set procedure for accomplishing this transformation. The simplest and most straight-forward procedure is to make this transformation using the scaling factor of the model. Since

$$1m|_m = 1920m|_p ,$$

one can write

$$\frac{\chi V}{Q_s} \Big|_p (m^{-2}) = \frac{1}{1920^2} \frac{\chi V}{Q_s} \Big|_m (m^{-2}) .$$

The sample scaling of the concentration parameter from model to field appears to give reasonable results. All data reported herein are in terms of the dimensionless value, $K = \frac{\chi V_a D^2}{Q_s}$.

-Errors in Concentration Measurement-

Each sample as it passes through the flame ionization detector, is separated from its neighbors by a period during which nitrogen flows. During this time, the detector is at its baseline, or zero level. When the sample passes through the

detector, the output rises to a value equal to the baseline plus a level proportional to the amount of tracer gas flowing through the detector. The baseline signal is set to zero and monitored for drift. Since the chromatograph used in this study features a temperature control on the flame and electrometer, there is very low drift. The integrator circuit is designed for linear response over the range considered.

A total system error can be evaluated by considering the standard deviation found for a set of measurements where a pre-calibrated gas mixture is monitored. For a gas of ~ 100 ppm propane ± 1 ppm, the average standard deviation from the electrometer was two per cent. Since the source gas was premixed to the appropriate molecular weight and repetitive measurements were made of its source strength, the confidence in source strength concentration is similar. The flow rate of the source gas was monitored by Fischer-Porter flow meters which are accurate to 2 per cent, including calibration and scale fraction error. The wind-tunnel velocity was constant to ± 10 per cent at such low settings. Hence, the cumulative confidence in the measured values of the dilution factor $(\frac{\chi V}{Q})_s$ will be a standard deviation of about ± 11 per cent, whereas the worst cumulative scenario suggests an error of no more than ± 20 per cent.

The lower limit of measurement is imposed by the instrument sensitivity and the background concentrations of hydrocarbons in the air within the wind tunnel. Background concentrations were measured and subtracted from all measurements quoted herein;

however, a lower limit of 1 to 2 ppm of propane is available as a result of background methane levels plus previous propane releases. An upper limit for propane with the instrument used is 10 per cent propane by volume. A recent report on the flame ionization detector for sampling gases in atmospheric wind tunnels prepared by Dear and Robins (1974) arrives at similar figures.

-Test Results: Concentration Measurements-

Since the conventional point-source diffusion equations cannot be used for predicting diffusion near objects which cause the wind to be nonuniform and nonhomogeneous in velocity and turbulence, it is necessary to calculate gaseous concentrations on the basis of experimental data. It is convenient to report dilution results in terms of a nondimensional factor independent of model to prototype scale.

In Cermak et al. (1966) and Halitsky (1963), the problem of similarity for diffusing plumes is discussed in detail. Considering this, the concentration measurements were transformed to K-isopleths by the formula

$$K = \frac{\chi V_a D^2}{Q_s}$$

where

χ = sample volume concentration,

D = cell diameter,

V_a = mean wind velocity at meteorological tower,

Q_s = gas source release rate (mass per unit time).

When interpreting model concentration measurements, it is important to remember that there can be considerable difference between the instantaneous concentration in a plume and the average concentration due to horizontal meandering. In the wind tunnel, a plume does not generally meander due to the absence of large-scale eddies. Thus, it is found that field measurements of peak concentrations which effectively eliminate horizontal meandering should correlate with the wind tunnel data (Hino, 1968). In order to compare downwind measurements of dispersion to predict average field concentrations, it is necessary to use data on peak-to-mean concentration ratios as gathered by Singer, et al. (1953, 1963). Their data is correlated in terms of the gustiness categories suggested by Pasquill for a variety of terrain conditions. It is possible to determine the frequency of different gustiness categories for a specific site. Direct use of wind tunnel data at points removed from the building cavity region may underestimate the dilution capacity of a site by a factor of four unless these adjustments are considered (Martin, 1965).

To estimate the equivalent prototype sampling time, another dimensionless variable was derived by including time as one of the pertinent parameters. The relation then exists

$$\left(\frac{\tau V_a}{L_o}\right)_m = \left(\frac{\tau V_a}{L_o}\right)_p \qquad \text{or,}$$

$$\tau_p = \tau_m \left(\frac{L_p}{L_m}\right) \left(\frac{V_{am}}{V_{ap}}\right) .$$

Since the model sampling time was approximately 30 s, then

$$\tau_p = \left(\frac{30}{60}\right)\left(\frac{1920}{1}\right)\left(\frac{7.2}{1920}\right)^{\frac{1}{2}} = 59 \text{ min.}$$

Since the prototype sampling time of interest is one hour, the data presented herein have not been corrected for sampling time.

3.5 Wind Profile Measurements

-Hot Wire Measurements-

Velocity measurements over the terrain model at various locations were obtained using hot-wire anemometry techniques.

A constant temperature TSI hot wire anemometer* was used for measuring both the root-mean-square value and the mean of the wind speed in the wind tunnel model. Calibration over the model was carried out in standard flow calibration tubes. The calibration measurements were correlated to King's law and put in the following form:

$$\frac{E^2}{R_h(R_h - R_c)} = A + BU^n$$

---

*Detailed discussion on hot-wire anemometry can be found in textbooks. Only those concepts that are essential to our measurements are presented here.

where

R_h = hot resistance of the wire

R_c = cold resistance of the wire

E = the output signal of the wire (mv)

U = the velocity sensed (m/s)

n, A and B = the constants of King's law.

Although the power n was found to be close to 0.5 over the velocity range 1.8 m/s to 152 m/s, it was found to be equal to 0.6694 at the low velocity range 0.03 m/s to 1.2 m/s. The King's law constants are thus

A = 0.266955

B = 0.036573

n = 0.6694.

Calibration data and results are shown in Table 3.5-1.

To obtain the velocity measurements, a calibrated carriage was used, together with a digital voltameter. In this manner, the location of the hot-wire probe over the terrain could be adjusted from outside the tunnel.

-Smoke-Wire Wind Profile Visualization-

The smoke-wire system was used to visualize instantaneous wind profiles. The smoke-wire probe (shown in Figure 3.5-2) is a tubular frame on which a nichrome wire 0.05 cm in diameter and approximately 66 cm long (1267 m in prototype) is held in a vertical position on insulated contacts. The wire, of about 325-ohm-per-foot resistance, is coated with a light oil, which, when heated, will rapidly evaporate

and form a line of smoke which moves with the air stream and traces the velocity profiles instanteously. The heating of the nichrome wire is accomplished by discharging a capacitor through it; the pulse of current from the capacitor (two micro-farad) causes rapid heating of the wire and vaporization of the oil. The trigger control circuit is adjusted to 1000 volts. The electronic pulse is also used to start a time counter.

The visualizations presented herein were taken with a 0.5-second delay; the smoke-wire probe was located at three different positions (denoted by S, A, and M in Figure 4.2-10) near Sites 1 and 2, at simulated elevations of 720, 793, and 976 m, MSL.

4.0 TEST PROGRAM RESULTS - SITE 1

4.1 Plume Visualization

The test results consist of photographs and movies showing Site 1 plume behavior for different wind directions and speeds. Of particular interest is the plume transport and dispersion in the vicinity of Anderson Springs.

The sequence of photographs in Figures 4.1-1, 4.1-2, and 4.1-3 shows plume behavior for the 210°, 230°, and 250° wind directions at meteorological tower height (10 m, AGL) and wind speeds of 3.2, 6.5, and 9.8 m/s for each direction. The plume behavior for each direction is generally the same. For the light wind speed cases (3.2 m/s) the plume tends to rise over Anderson Springs. However, as the wind speed increases, the plume altitude decreases, and for the high wind speed cases, the plume tends to follow along the terrain confluences.

For wind directions of 210°, 230° and wind speeds of 6.5, and 9.8 m/s, the plume emanating from the cooling tower appears to flow over Anderson Springs at a relatively low effective plume altitude. No obvious plume transport toward Whispering Pines was observed for the wind directions considered.

Complete sets of still photographs supplement this report. Color motion pictures have been arranged into titled sequences and the sets available are given by run number in Table 4.1-1.

4.2 Concentration Measurements

The diffusion of gaseous effluent emitted from a model cooling tower located at Site 1 was studied for three wind directions

(210°, 230°, and 250° azimuth) and three wind speeds for each direction (3.2, 6.5, and 9.8 m/s). Propane concentrations at ground level were measured at distances from 600 to 3000 m downwind.

For each wind direction studied, thirty-four gas samples were collected at ground level. The sampling arrays for the three wind directions are shown in Figure 4.2-10, 4.2-11, and 4.2-12. The prototype locations for all sampling points are summarized in Table 4.2-4 with north and east as positive directions. The zero coordinate is the center of the terrain which was mounted on the turntable. This point is represented by the base of the wind direction arrow in all figures.

All concentration data have been reported in dimensionless form as explained in Section 3.4. To convert from a dimensionless concentration coefficient, K, to a prototype H_2S concentration, refer to the procedure outlined in Appendix A.

The results for the wind directions and speeds studied are presented in Tables 4.2-1, 4.2-2, and 4.2-3. Sample locations in the tables are defined in Table 4.2-4, and Figures 4.2-10, 4.2-11, and 4.2-12.

In order to visually and quantitatively assess the effect of wind direction and wind speed on ground level concentration patterns, Figure 4.2-1 through 4.2-9 were prepared. These figures show isopleths for the dimensionless concentration coefficient, K, for the wind directions and speeds studied. These figures clearly

show the expected increase in maximum ground level concentration with increased wind speed. Additionally, the figures generally show that the maximum values move closer to the source as the wind speed increases.

The highest K-value near Anderson Springs of 53.0 was observed to occur with a 210° wind direction at 9.8 m/s. Figure 4.2-3 shows the isopleth pattern for this case. At this speed and direction, it is evident that the plume is mixed rapidly to the ground after emission and follows the terrain confluences down through Anderson Springs. This same pattern is evident for the other high wind speed case except the plume transport is not as close to Anderson Springs.

The K-isopleths for the 3.2 m/s cases are all near the background value and consequently the absolute values have a larger error than for the 6.5 and 9.8 m/s cases. Regardless, the values for the light wind cases are low and near zero.

5.0 TEST PROGRAM RESULTS - SITE 2

5.1 Plume Visualization

The test results consist of photographs and movies showing Site 2 plume behavior for different wind directions and speeds. Of particular interest is the plume transport and dispersion in the vicinity of Anderson Springs.

The sequence of photographs in Figure 5.1-1, 5.1-2, and 5.1-3 shows plume behavior for the 210°, 230°, and 250° wind directions and speeds at meteorological tower height (10 m, AGL) of 3.2, 6.5, and 9.8 m/s for each direction. The plume behavior for each direction is generally the same. For the light wind speed cases, (3.2 m/s), the plume tends to rise over Anderson Springs. However, as the wind speed increases, the plume altitude decreases and for the high wind speed cases tends to follow along the terrain confluences.

For wind directions of 210° and 230° and wind speeds of 6.5 and 9.8 m/s, the plume emanating from the cooling tower appears to flow over Anderson Springs at a relatively low effective plume altitude. No obvious plume transport toward Whispering Pines was observed for the wind directions considered.

Complete sets of still photographs supplement this report. Color motion pictures have been arranged into titled sequences and the sets available are summarized by run number in Table 5.1-1.

5.2 Concentration Measurements

The diffusion of gaseous effluent emitted from a model cooling tower located at Site 2 was studied for three wind directions (210°, 230°, and 250° azimuth) and three wind speeds for each direction

(3.2, 6.5, and 9.8 m/s). Propane concentrations at ground level were measured at distances from 1200 to 3600 meters downwind.

For each wind direction studied, thirty-four gas samples were collected at ground level. The sampling arrays for the three wind directions are shown in Figures 4.2-10, 4.2-11, and 4.2-12. The prototype locations for all sampling points are summarized in Table 4.2-4 with north and east as positive directions. The zero coordinate is the center of the terrain which was mounted on the turntable. This point is represented by the base of the north arrow in all figures.

All concentration data have been reported in dimensionless form as explained in Section 3.4. To convert from a dimensionless concentration coefficient, K, to a prototype H_2S concentration, refer to the procedure outlined in Appendix A.

The results for the wind directions and speeds studied are presented in Tables 5.2-1, 5.2-2, and 5.2-3. Sample locations in the tables are defined in Table 4.2-4 and Figures 4.2-10, 4.2-11, and 4.2-12.

In order to visually and quantitatively assess the effect of wind direction and wind speed on ground-level concentration patterns, Figures 5.2-1 through 5.2-9 were prepared. These figures show isopleths of the dimensionless concentration coefficient, K, for the wind directions and speeds studied. These figures clearly show the expected increase in maximum ground-level concentration with increased wind speed. Additionally, the figures generally show that the maximum values move closer to the source as the wind speed increases.

The highest K-value near Anderson Springs of 37.3 was observed to occur with a 230° wind direction at 13.4 m/s. Figure 5.2-6 shows the isopleth pattern for this case. At this speed and direction, it is evident that the plume is mixed rapidly to the ground after emission and follows the terrain confluences down through Anderson Springs. This same pattern is evident for the other high wind speed case except the plume transport is not as close to Anderson Springs.

The K-isopleths for the 3.2 m/s cases are all near the background value and consequently, the absolute values have a larger error than for the 6.5 and 9.8 m/s cases. Regardless, the values for the light-wind cases are low and near zero.

6.0 TEST RESULTS - VELOCITY MEASUREMENTS

This section discusses the results of the velocity measurements. Techniques for data collection are described in Section 3.5. Both the mean value and the root mean square of wind speed were measured in the wind tunnel.

The turbulence intensities $\frac{V_{rms}}{V}$ are plotted in Figure 6-1 for Sites 1 and 6. As a general trend, the turbulence intensity is higher near the ground. The two sites have nearly the same turbulence intensity up to 0.01 m from the ground (this corresponds to 24 m from the ground in the prototype). The values of the turbulence intensity appear to be about 1.2 times higher at Site 1 than at Site 6 over heights of 73 m to 488 m above the terrain. At higher levels, the effect of the terrain appears to be negligible and both sites have nearly the same root mean square value of wind velocity.

Figure 6-2 shows the mean wind-velocity profiles at Sites 1 and 6. The mean velocity at the low levels ($z < 488$ m, AGL) appears to have higher values at Site 6 than at Site 1. The power-law fit to the wind profiles for the two locations using the following equation,

$$\frac{V}{V_\infty} = \frac{z}{z_\infty}^{1/n}$$

gives the following values for 1/n:

$1/n \cong 0.12$ Site 6

$1/n \cong 0.176$ Site 1.

These values compare favorably with the 1/7-power law for neutral flow ($1/n = 0.14$). Using the power-law relations, the velocity at three

heights above ground level (10, 20, and 40 m) were computed for the two sites. The values are enumerated in Table 6-1, illustrating that Site 6 has the greatest speeds at these heights.

Figure 6-3 (showing constant velocity lines over the terrain) illustrates the acceleration of the velocity on the top and downwind side of the ridge. Also evident is the general downward air motion which greatly affects plume transport.

The smoke-wire visualization at three levels for a low free-stream wind velocity of 0.13 m/s in the model (corresponding to 2.15 m/s in the prototype) are shown in Figure 6-4. The three profiles in each photograph represent three intervals of time (each of 0.5 seconds long). The higher intensities of turbulence at the low levels with respect to the terrain are evident.

REFERENCES

Cermak, J. E. and J. Peterka, "Simulation of Wind Fields over Point Arguello, California, by Wind-Tunnel Flow over a Topographical Model," Final Report, U. S. Navy Contract N126(61756)34361 A(PMR), Colorado State University, CER65JEC-JAP64, December, 1966.

Cermak, J. E., "Laboratory Simulation of the Atmospheric Boundary Layer," AIAA Jl., Vol. 9, No. 9, pp. 1746-1754, September, 1971.

Cermak, J. E., V. A. Sandborn, E. J. Plate, G. J. Binder, H. Chuang, R. N. Meroney and S. Ito, "Simulation of Atmospheric Motion by Wind-Tunnel Flows," Colorado State University, CER66JEC-VAS-EJP-HC-RNM-SII7.

Cermak, J. E., "Applications of Fluid Mechanics to Wind Engineering," 1974 Freeman Scholar Lecture, ASME Journal of Fluids Engineering, Vol. 97, Series 1, No. 1, March, 1975, CEP74-75JEC7.

Dear, D. J. A. and A. G. Robins, "A Technique Used to Study the Dispersion of Gases in the MEL 9.14 m X 2.74 m Wind Tunnel," Central Electric Generating Board Report R/M/N752, United Kingdom, 1974.

Field, J. H. and R. Warden, "A Survey of the Air Currents in the Bay of Gibralter, 1929-1930," Air Ministry, Geophysical Memorandum No. 50, London, 1933.

Halitsky, J., J. Golden, P. Halpern and P. Wu, "Wind Tunnel Tests of Gas Diffusion from a Leak in the Shell of a Nuclear Power Reactor and from a Nearby Stack," Geophysical Sciences Laboratory Report No. 63-2, New York University, April, 1963.

Halitsky, J., "Gas Diffusion near Buildings," Geophysical Sciences Laboratory Report No. 63-3, New York University, February, 1963.

Hino, M., "Maximum Ground-Level Concentration and Sampling Time," Atmospheric Environment, Vol. 2, pp. 149-165, 1968.

Martin, J. E., "The Correlation of Wind Tunnel and Field Measurements of Gas Diffusion Using Kr-85 as a Tracer," Ph.D. Thesis, MMPP 272, University of Michigan, June, 1965.

Meroney, R. N. and J. E. Cermak, "Wind Tunnel Modeling of Flow Diffusion over San Nicolas Island, California," U. S. Navy Contract No. N123(61756)50192 A(PMR), Colorado State University, CER66-67RNM-JEC44, September, 1967.

Schlichting, H., Boundary Layer Theory, McGraw-Hill, New York, 1960.

Singer, I. A., I. Kazukiko and G. D. Roman, "Peak to Mean Pollutant Concentration Ratios for Various Terrain and Vegetative Cover," Journal of APCA, Vol. 13, No. 1, p. 40, 1963.

Singer, I. A. and M. E. Smith, "The Relation of Gustiness to Other Meteorological Parameters," Journal of Meteorology, Vol. 10, No. 2, 1953.

Turner, P. B., "Workbook of Atmospheric Dispersion Estimates," U. S. Department of Health, Education and Welfare, Public Health Service, Cincinnati, Ohio, 1969.

APPENDIX A

Method for Calculating Prototype Concentrations From Nondimensional Concentration Coefficient K

- Basic Equation:

$$K = \frac{\chi V_a D^2}{\Lambda Q_s} \quad \text{Prototype}$$

where

$K \equiv$ nondimensional concentration coefficient from wind tunnel study

$\chi \equiv$ H_2S concentration (ppm)

$V_a \equiv$ wind speed at the meteorological station (m/s)

$D \equiv$ cell diameter (equal to 8.5 m)

$\Lambda \equiv$ total volume flow (use 4313 m^3/s)

$Q_s \equiv$ equivalent H_2S concentration in the incoming stack gas [(ppm)(1 - fraction removed)]

- Now Solving for $\chi_{prototype}$:

$$\chi_{prototype} = K \frac{\Lambda Q_s}{V_a D^2}$$

$$= 59.69 \frac{KQ_s}{V_a}$$

- Example:

let $K = 20 \times 10^{-5}$

$Q_s = 100$ ppm

$V_a = 9.8$ m/s

then $\chi_{prototype} = \frac{(59.59)(20 \times 10^{-5})(100)}{9.8} = 0.12$ ppm

APPENDIX B

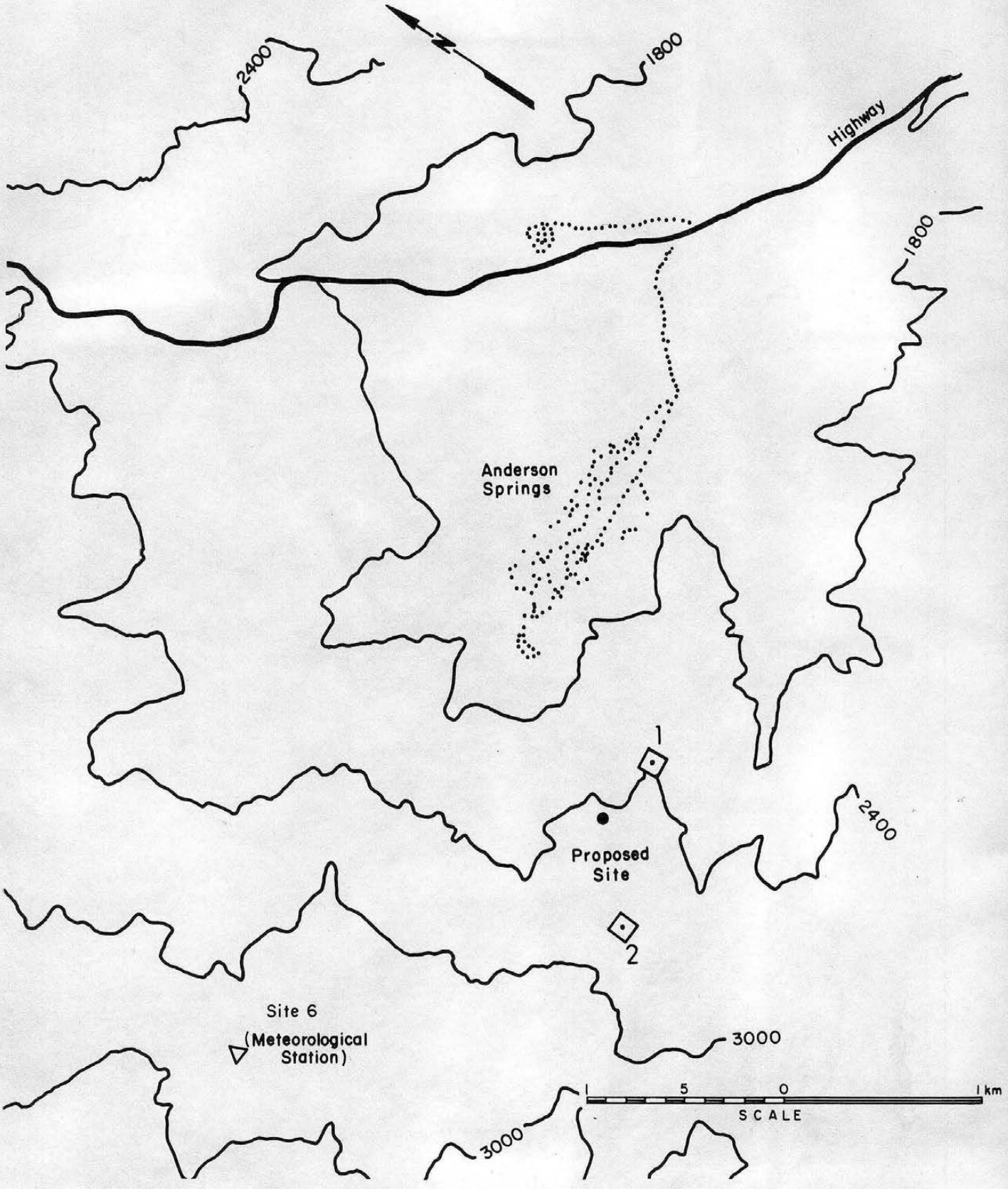

Figure 1.1 Map showing geyser geothermal area and location of proposed geothermal power plant Sites 1 and 2 for Unit 16 (1 inch = 610 m).

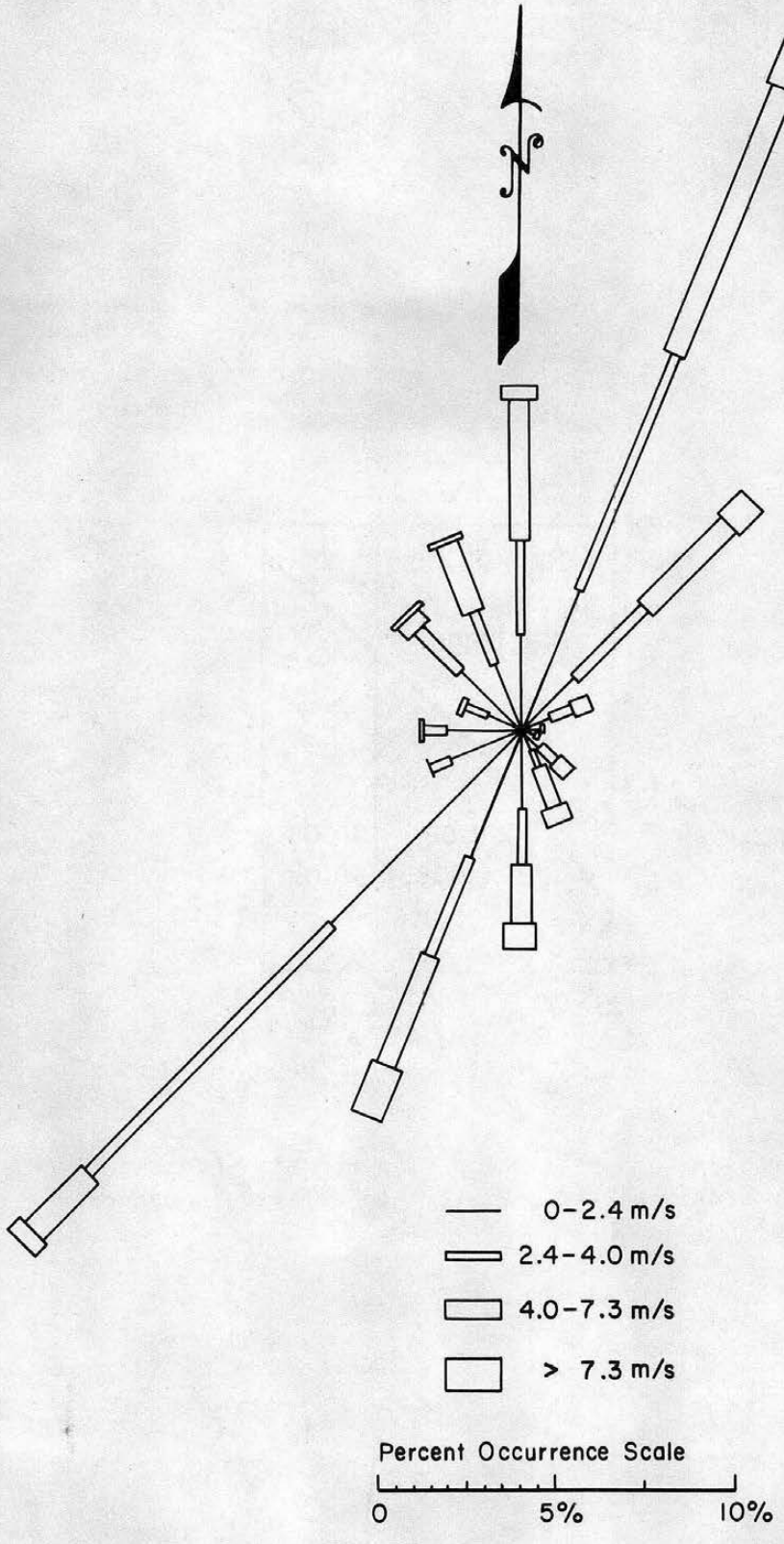

Figure 1.2 Wind rose from meteorological station located near proposed site.

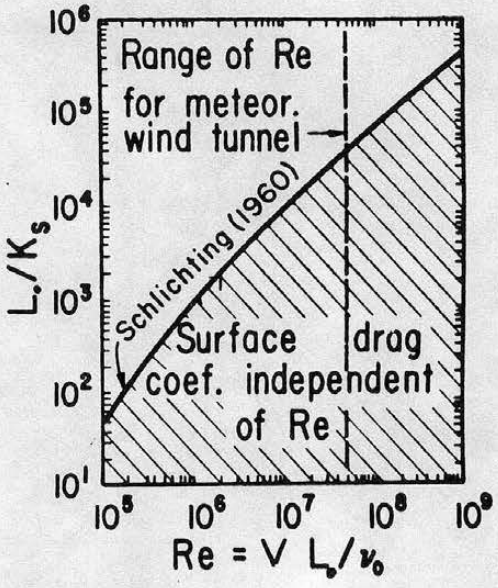

Fig. 2.1 Reynolds Number at which Flow Becomes Independent of Reynolds Number for Prescribed Relative Roughness

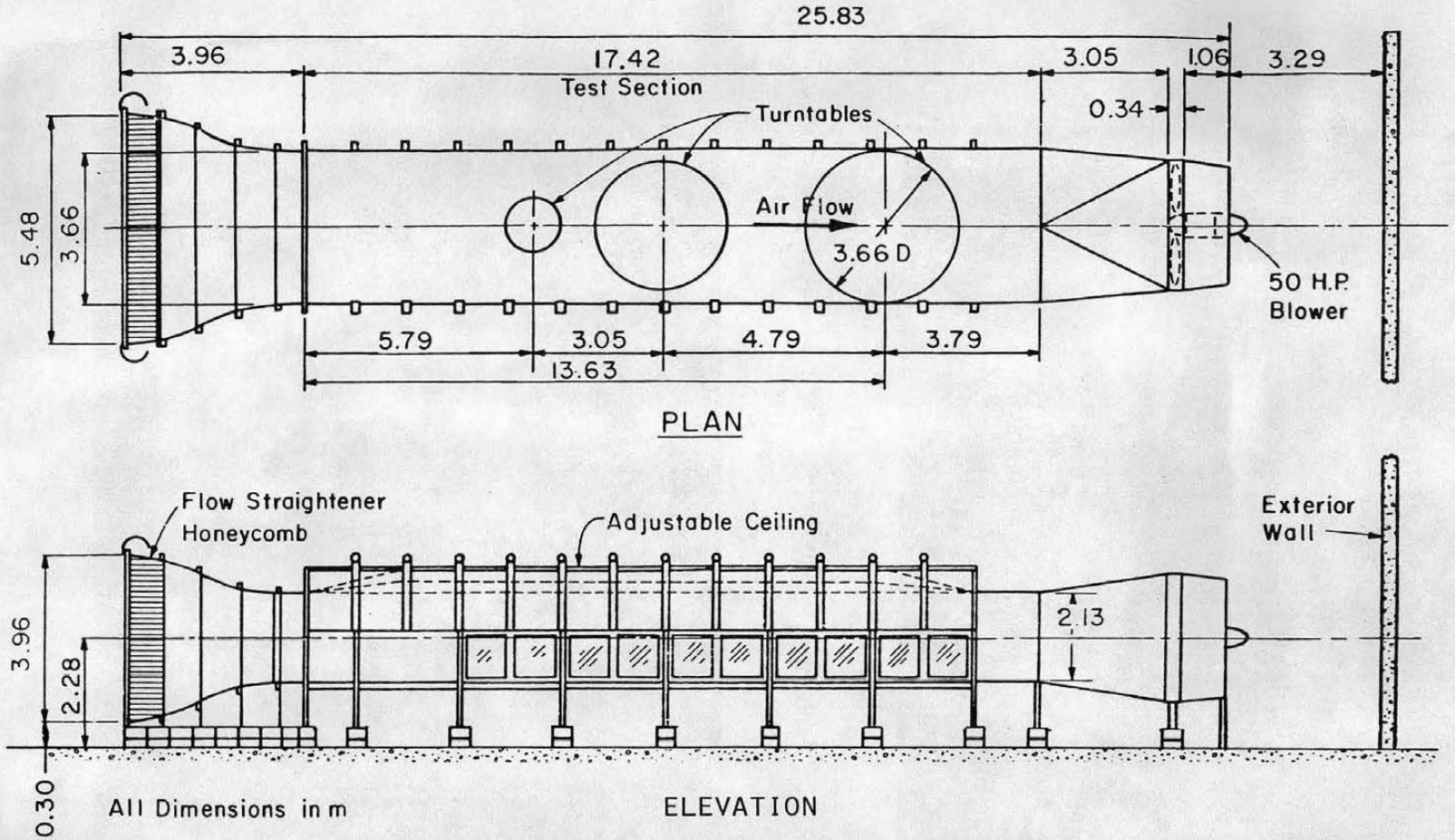

Figure 3.1-1 Environmental Wind Tunnel

FLUID DYNAMICS & DIFFUSION LABORATORY

COLORADO STATE UNIVERSITY

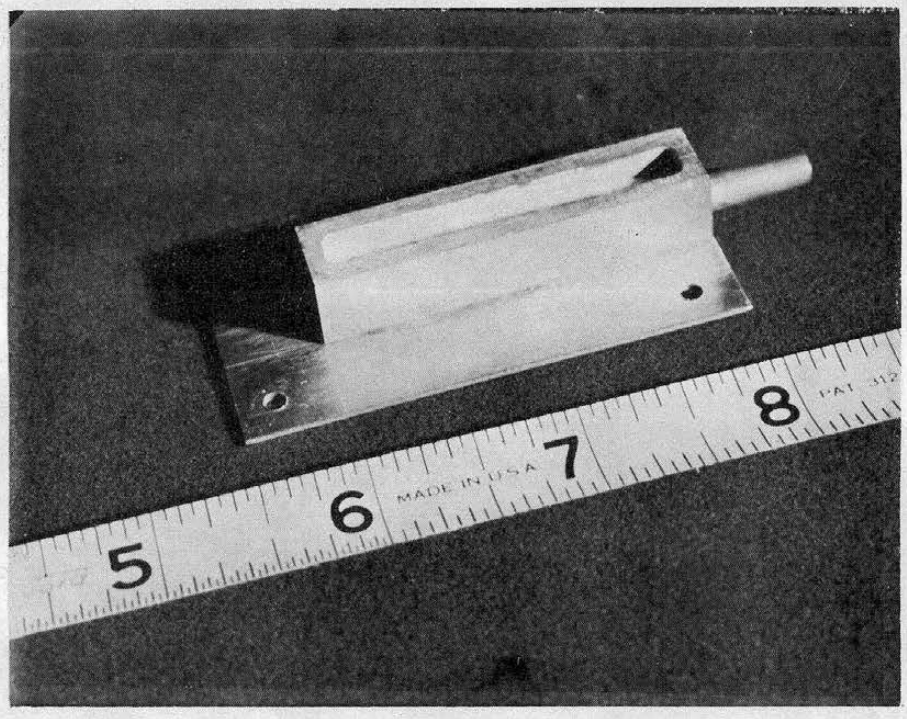

Figure 3.2-1 Photograph of Cooling Tower Model (Scale 1:1920)

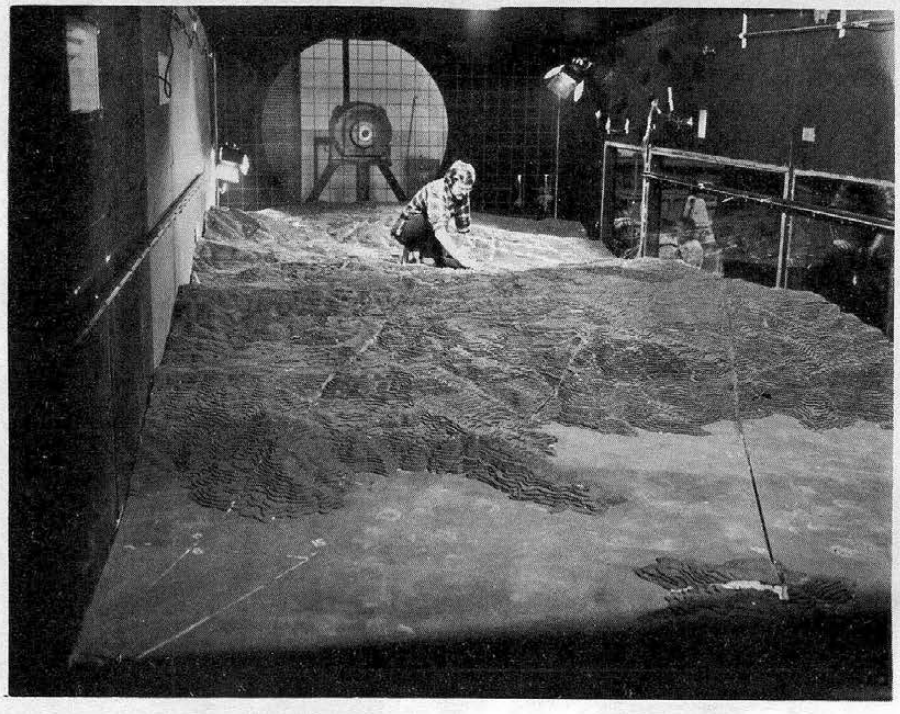

Figure 3.2-2 Photograph of Terrain Model in the Environmental Wind Tunnel

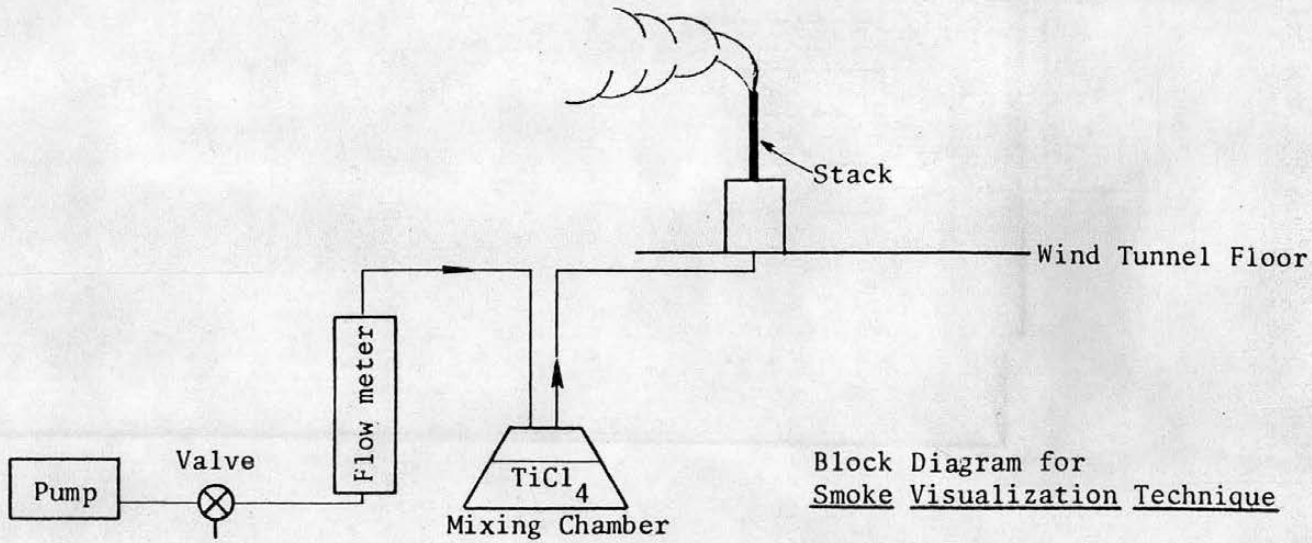

Figure 3.3-1 Schematic of plume visualization equipment.

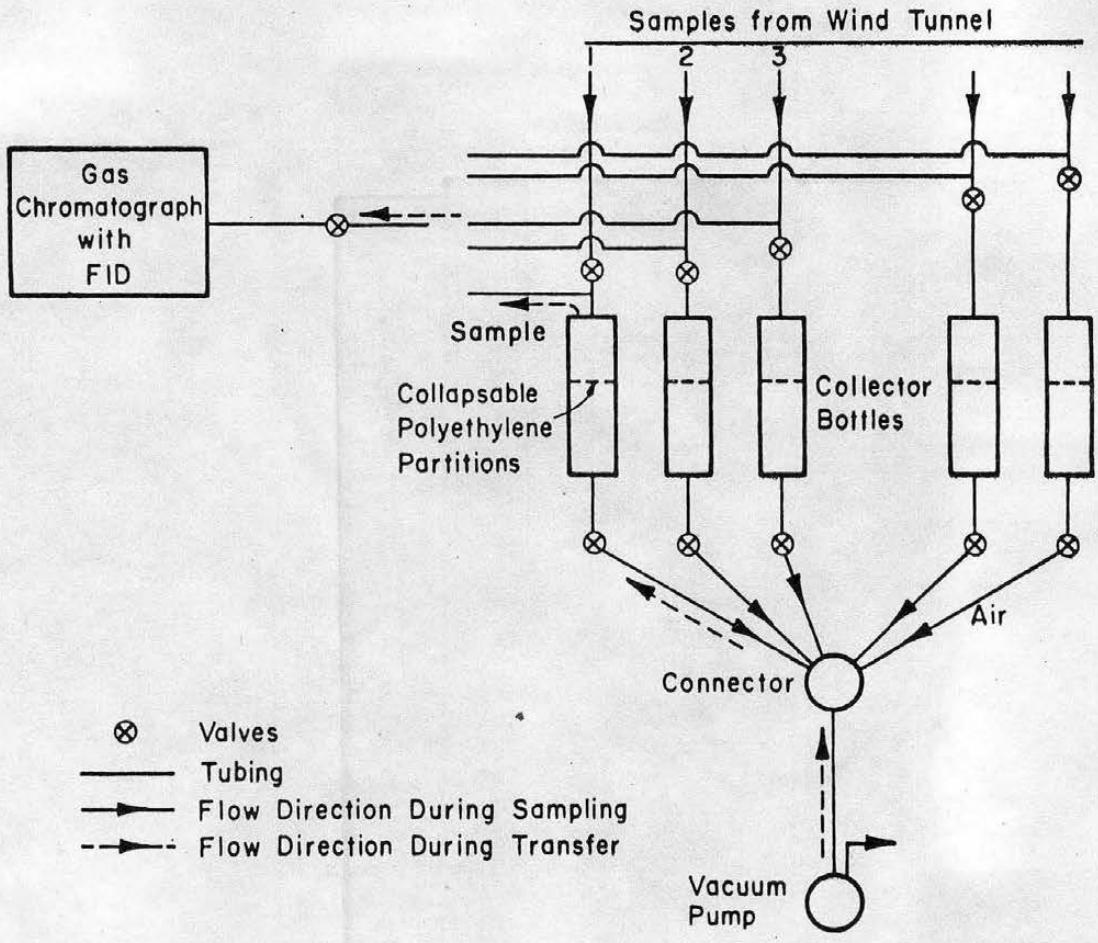

Figure 3.4-1 Schematic of tracer gas sampling system.

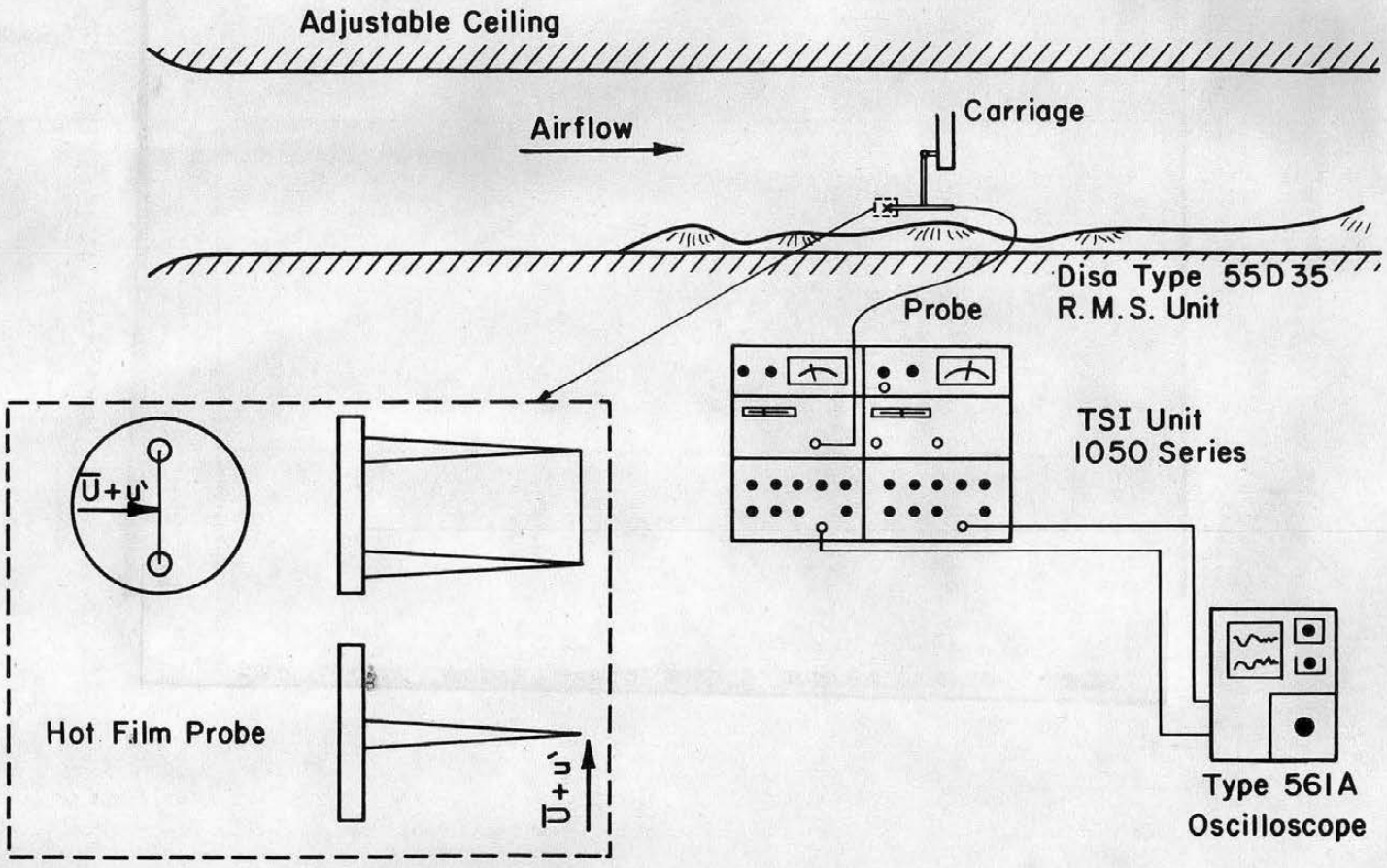

Figure 3.5-1 Laboratory experimental arrangement for obtaining turbulent intensities and mean wind velocities over the terrain.

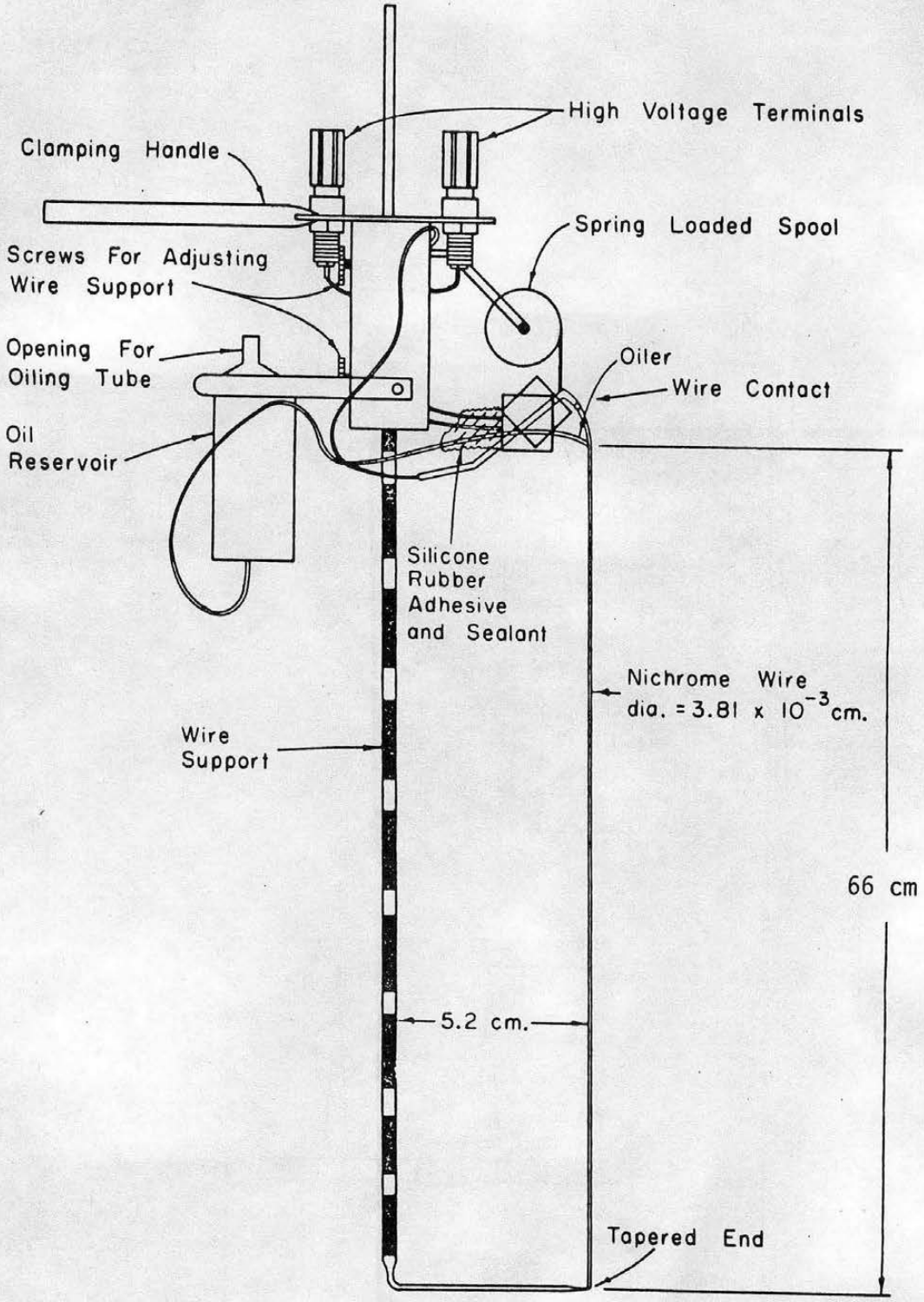

Figure 3.5-2 The Smoke-Wire Used to Visualize Wind Profiles Over the Terrain

Figure 4.1-1

Plume visualization of Unit 16 - Site #1 for Wind Direction 250° and a Wind Speed of

a) 3.2 m/s →

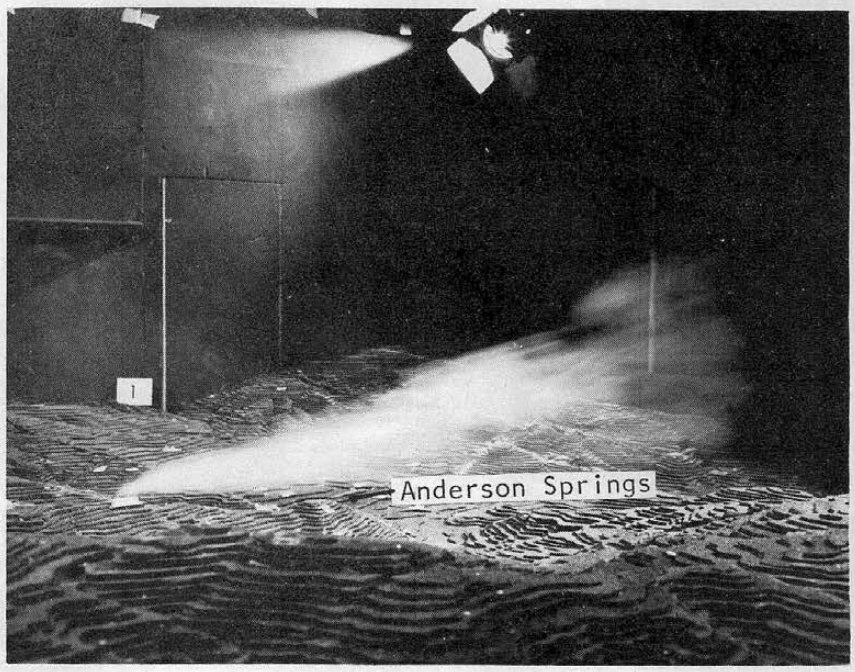

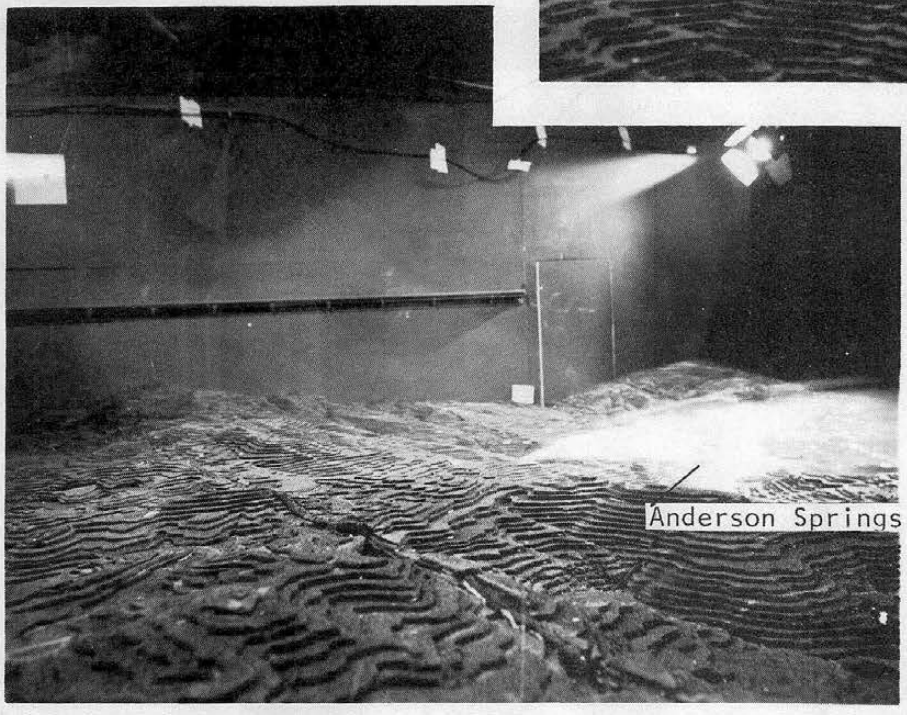

← b) 6.5 m/s

c) 9.8 m/s →

Figure 4.1-2

Plume visualization of Unit 16 - Site #1 for Wind Direction 230° and a Wind Speed of

a) 3.2 m/s →

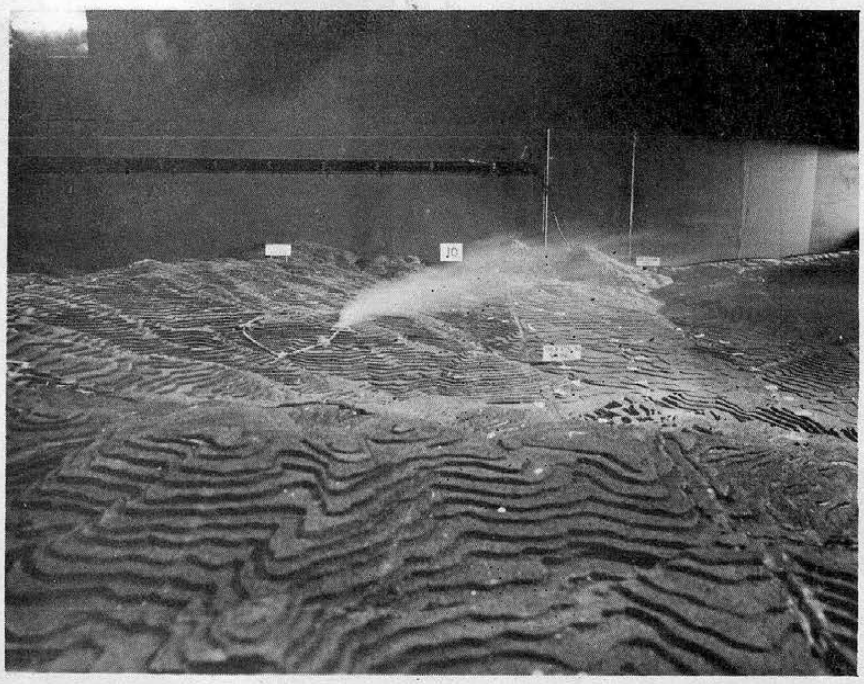

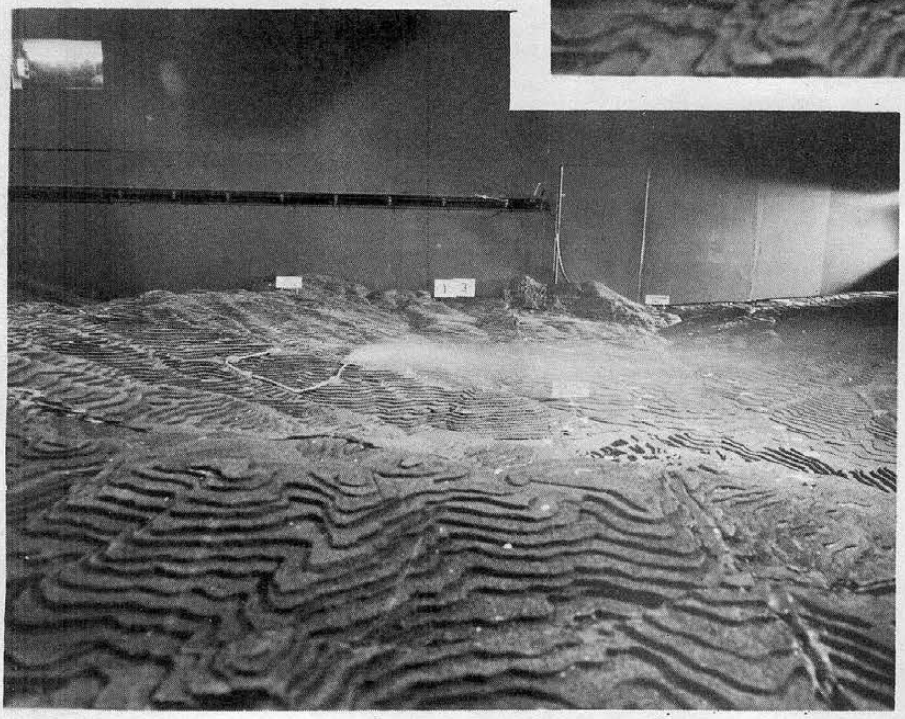

← b) 6.5 m/s

c) 9.8 m/s →

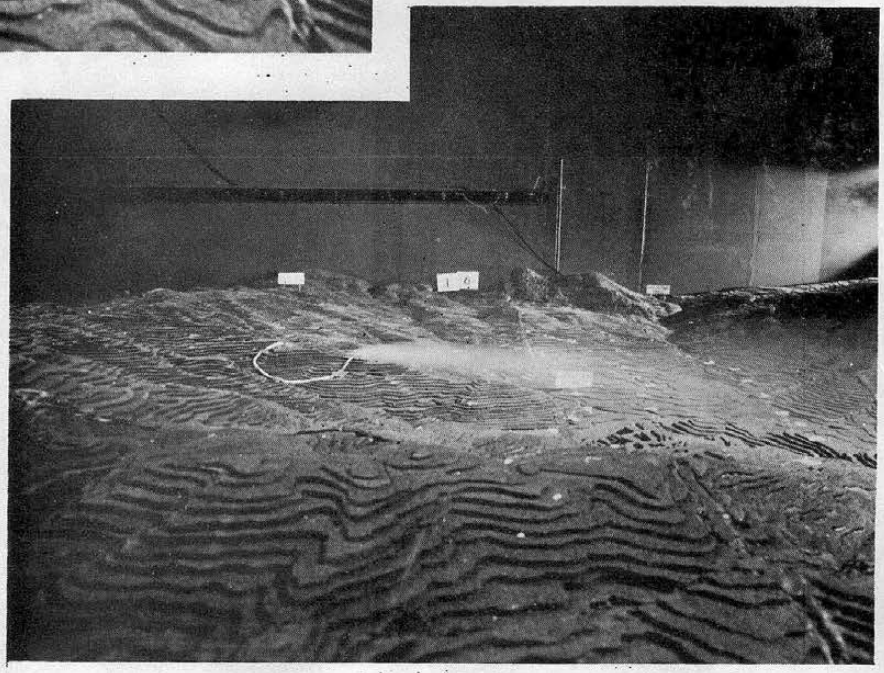

Figure 4.1-3

Plume visualization for Unit 16 - Site #1 for Wind Direction 210° and a Wind Speed of

a) 3.2 m/s →

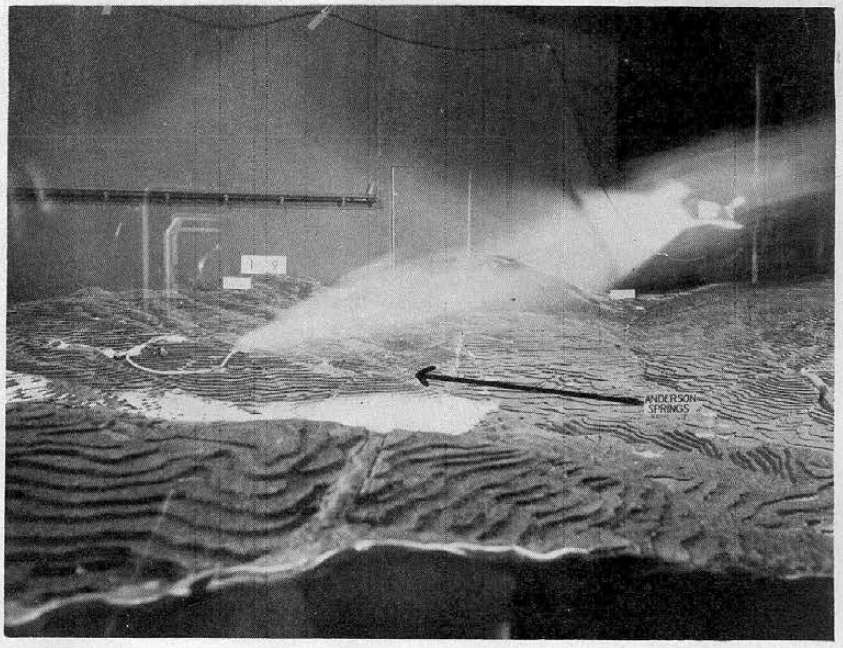

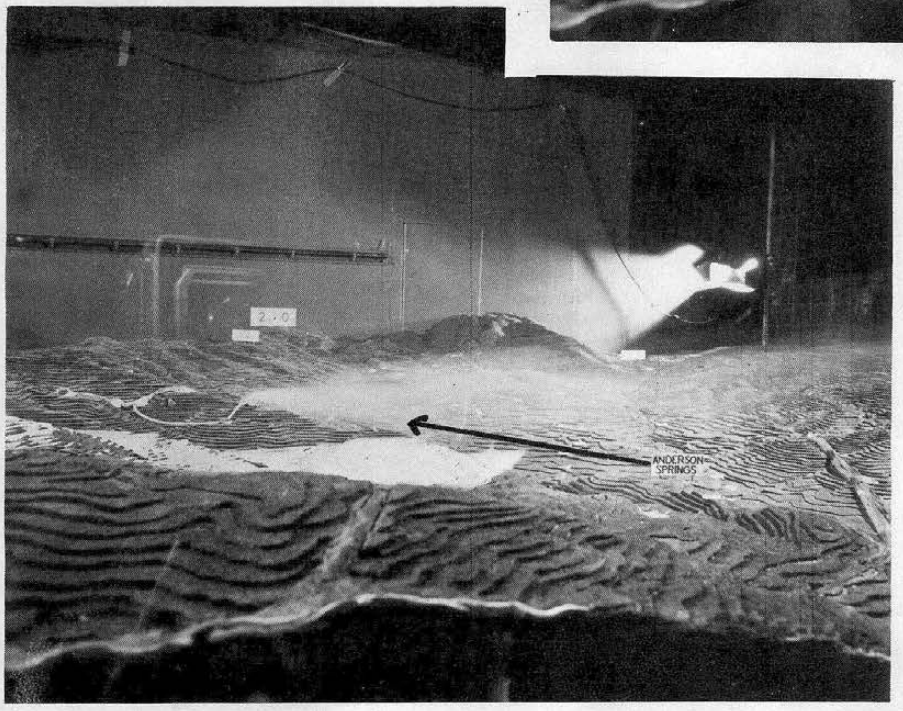

← b) 6.5 m/s

c) 9.8 m/s →

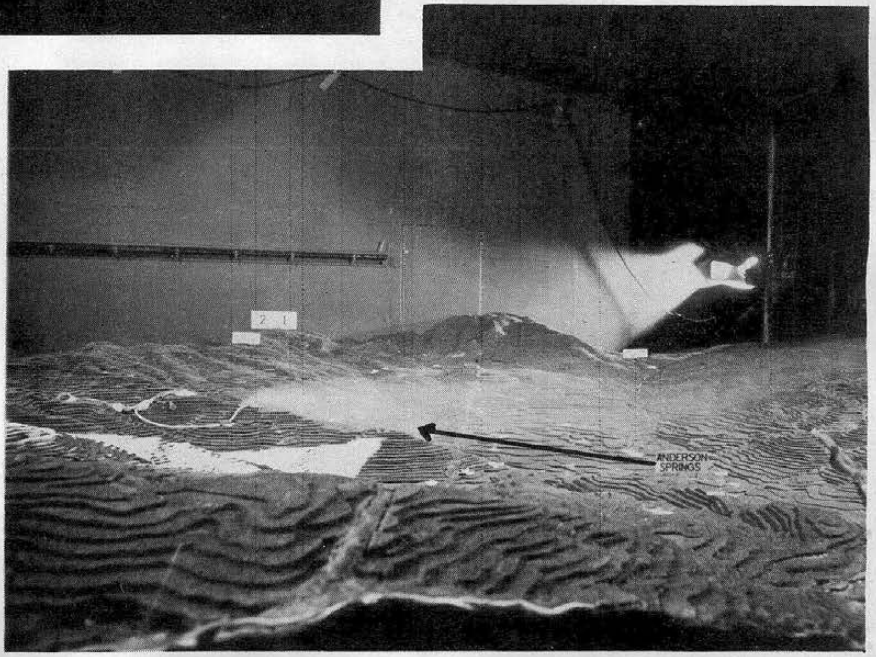

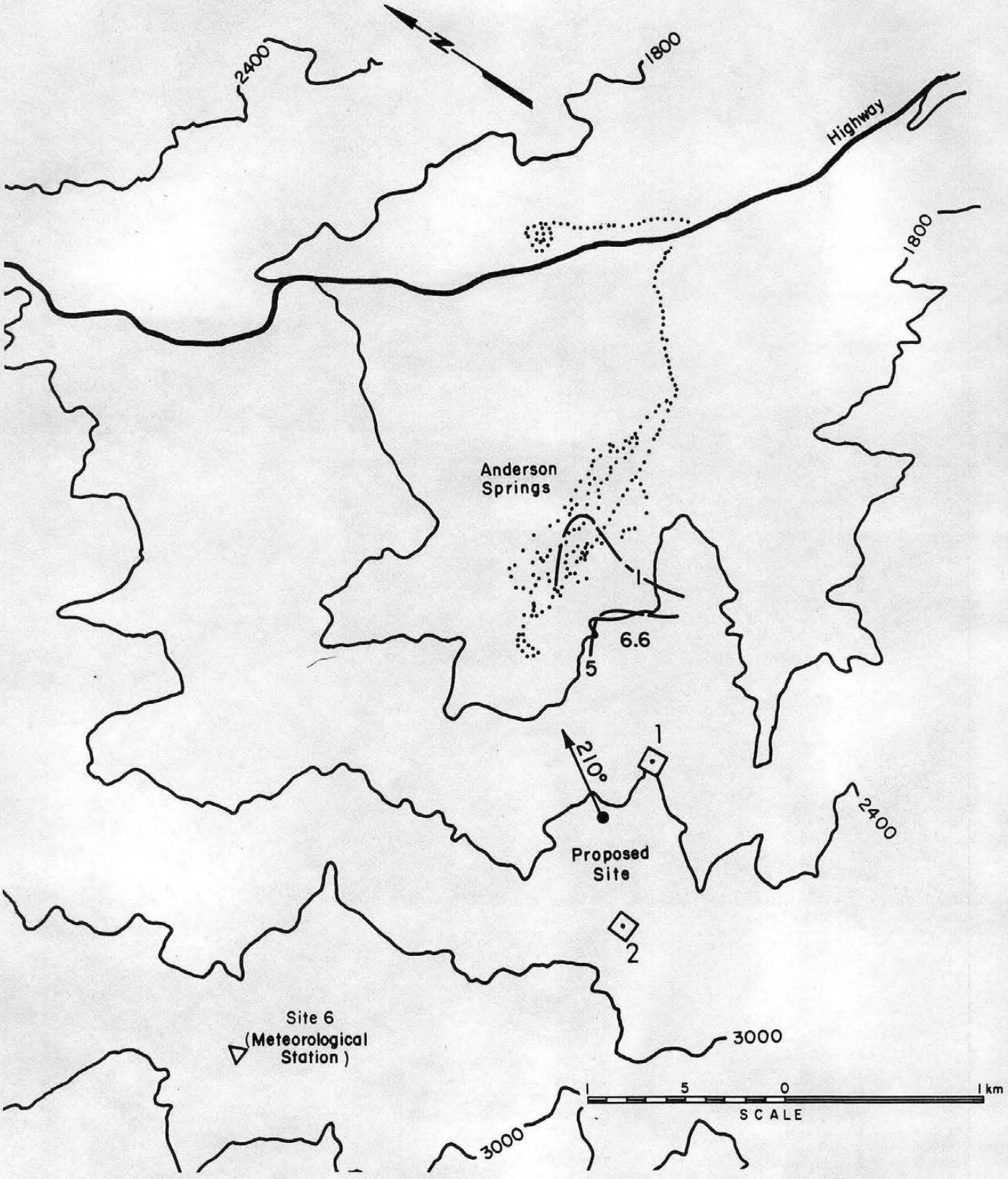

Figure 4.2-1 Isopleths of nondimensional concentration coefficient K (x 10^5) for Unit 16 - Site 1, wind direction 210°, and a wind speed of 3.2 m/s. (1 in = 610 m)

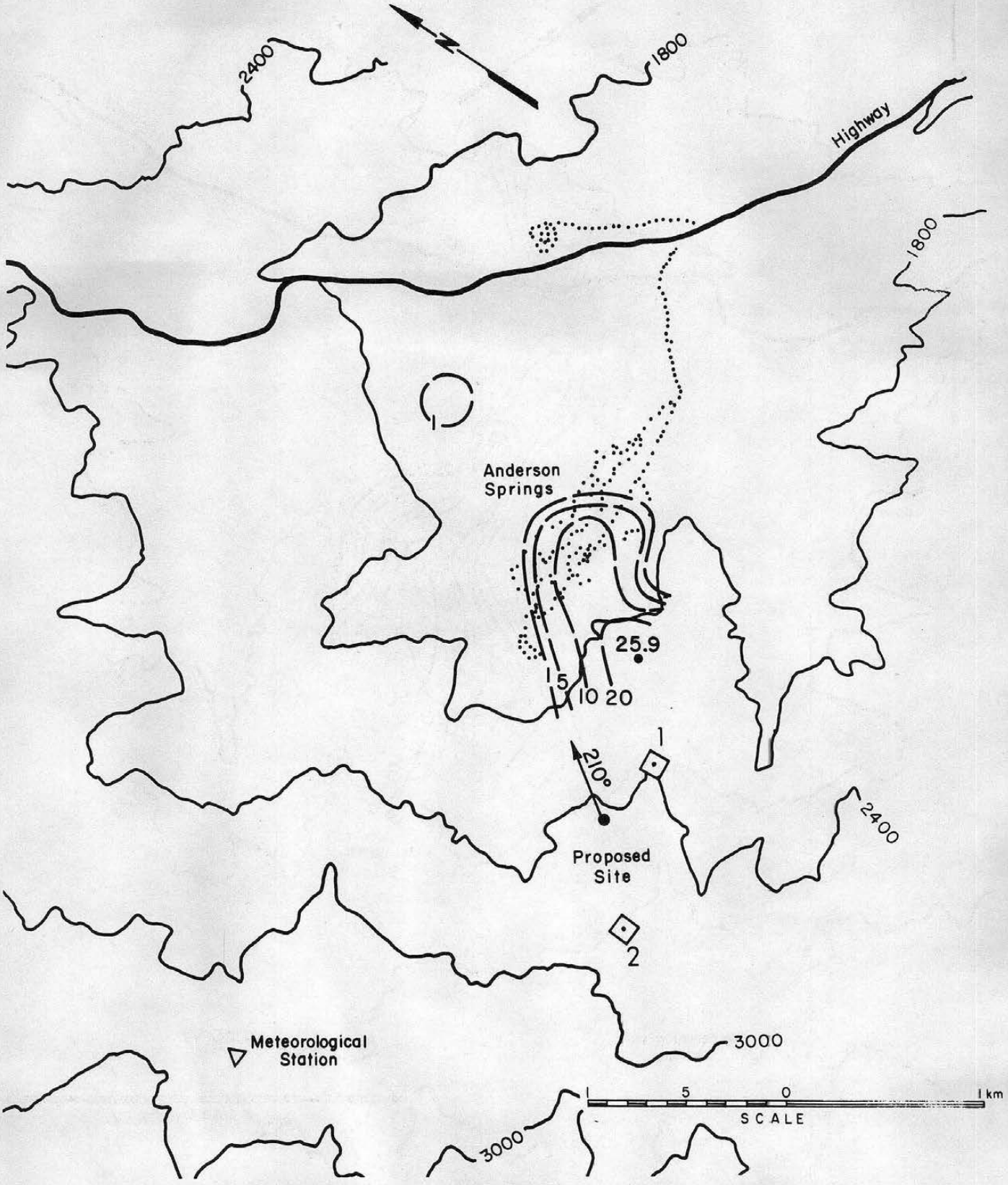

Figure 4.2-2 Isopleths of nondimensional concentration coefficient K (x 10^5) for Unit 16 - Site 1, wind direction 210°, and a wind speed of 6.5 m/s. (1 in = 610 m)

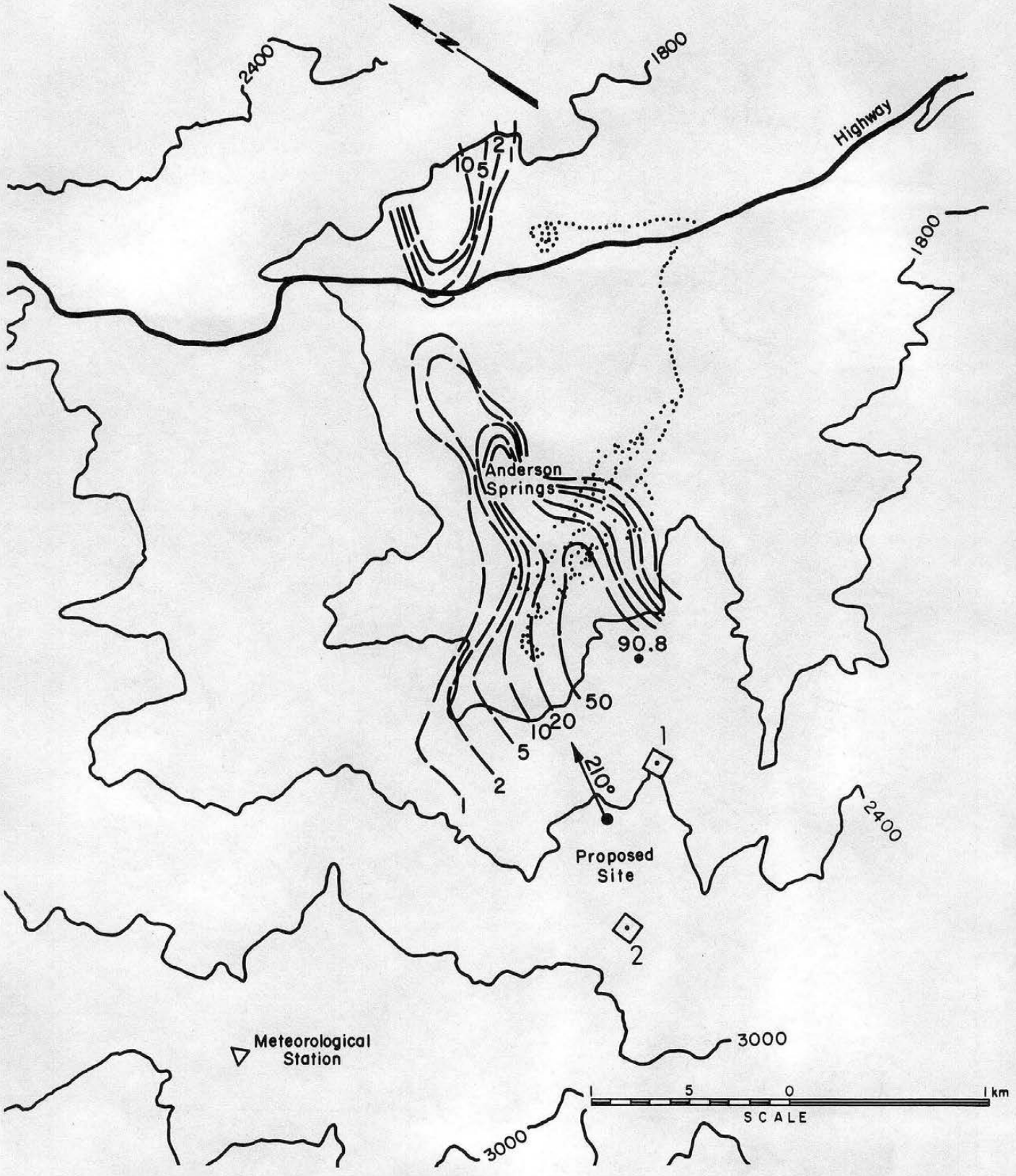

Figure 4.2-3 Isopleths of nondimensional concentration coefficient K (x 10^5) for Unit 16 - Site 1, wind direction 210°, and a wind speed of 9.8 m/s. (1 in = 610 m)

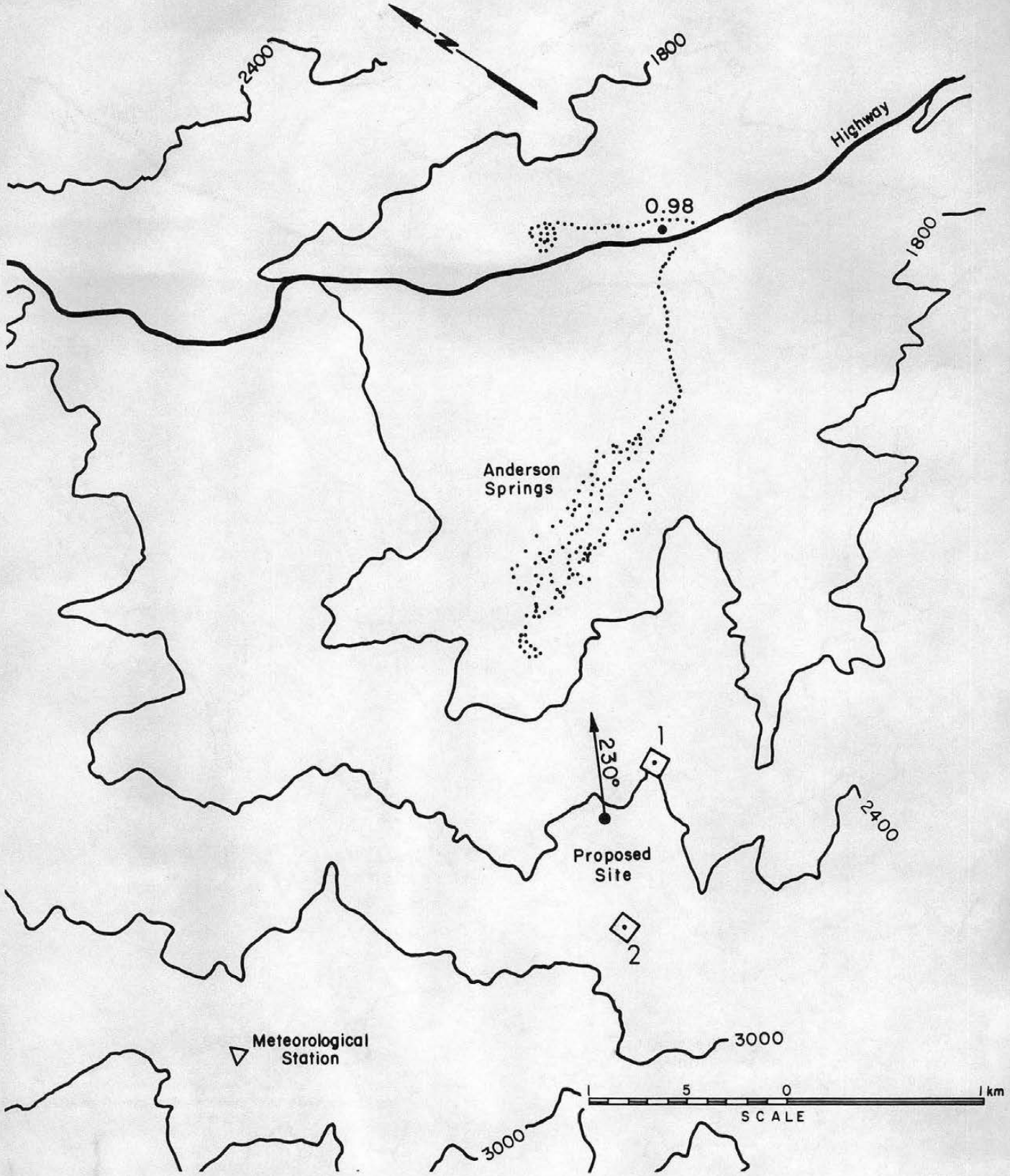

Figure 4.2-4 Isopleths of nondimensional concentration coefficient K (x 10^5) for Unit 16 - Site 1, wind direction 230°, and a wind speed of 3.2 m/s. (1 in = 610 m)

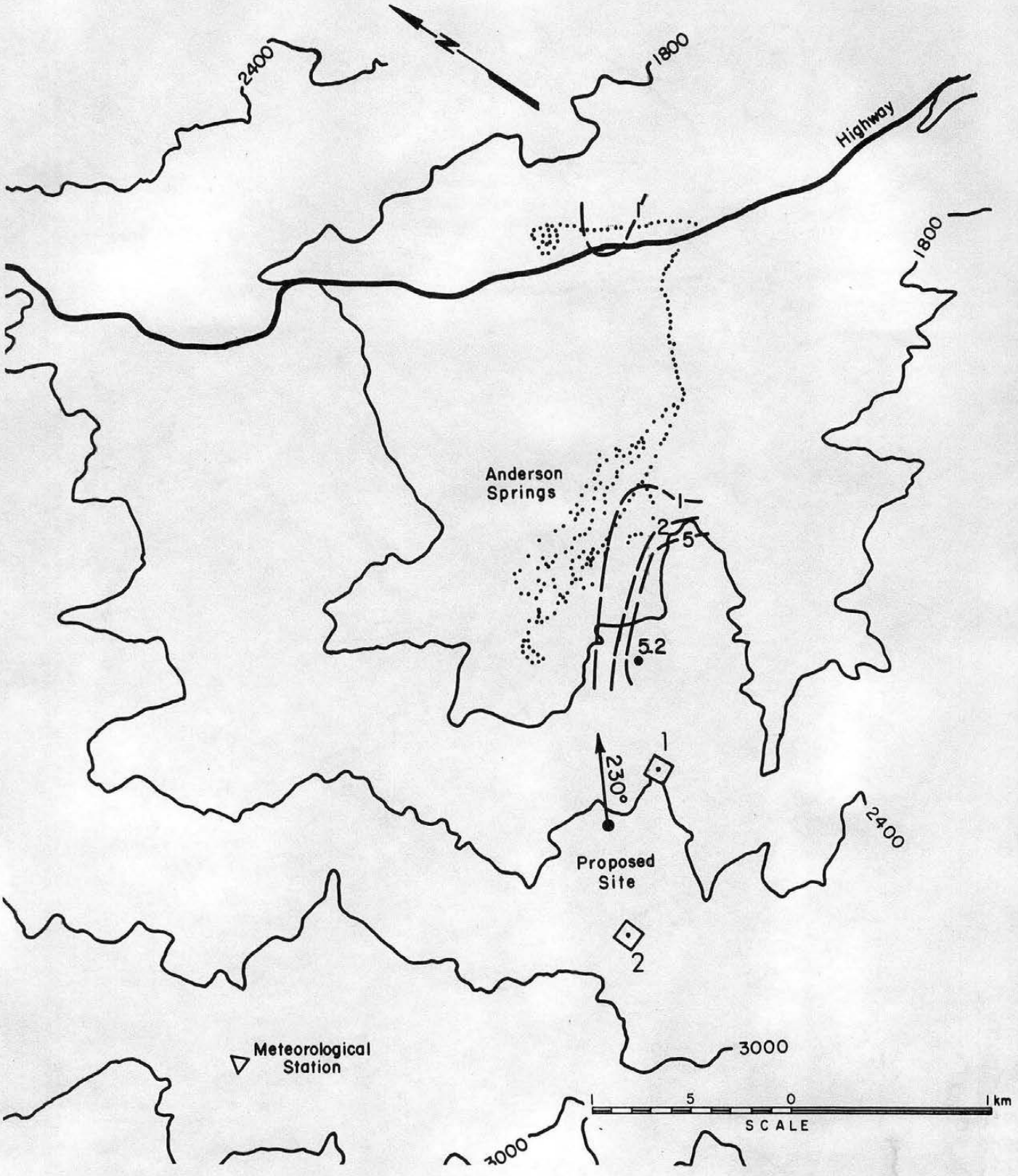

Figure 4.2-5 Isopleths of nondimensional concentration coefficient K (x 10^5) for Unit 16 - Site 1, wind direction 230°, and a wind speed of 6.5 m/s. (1 in = 610 m)

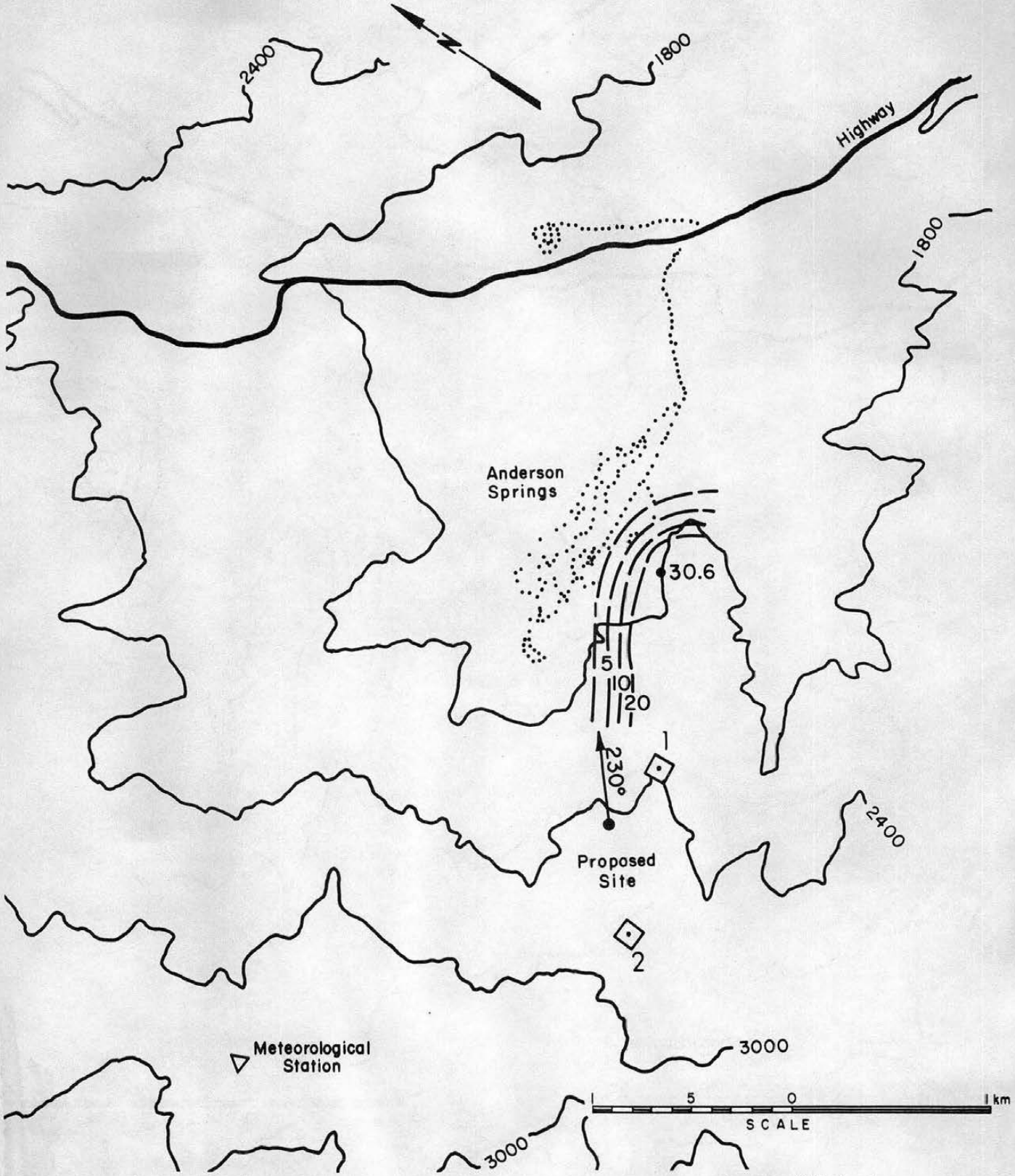

Figure 4.2-6 Isopleths of nondimensional concentration coefficient K (x 10^5) for Unit 16 - Site 1, wind direction 230°, and a wind speed of 9.8 m/s. (1 in = 610 m)

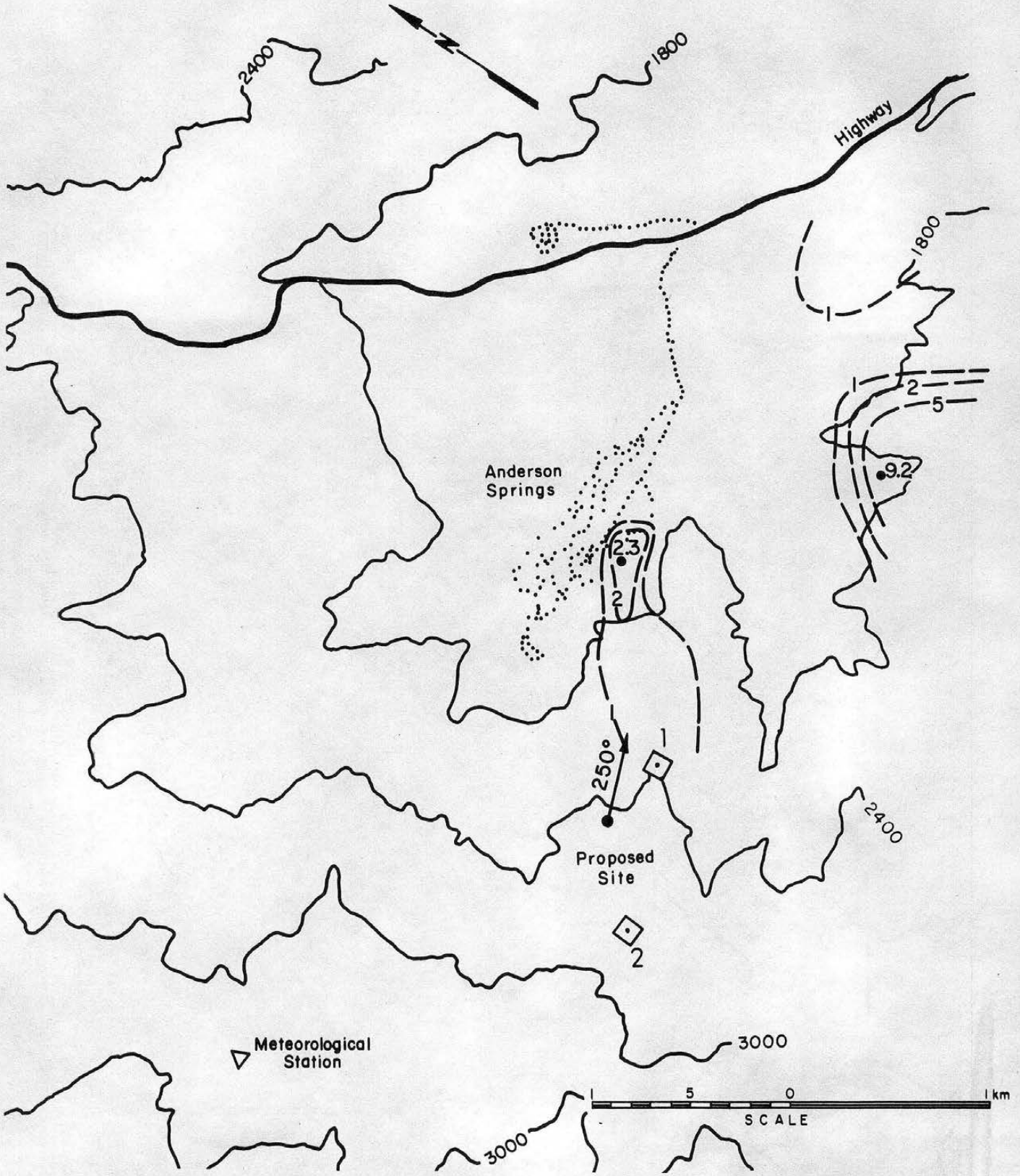

Figure 4.2-7 Isopleths of nondimensional concentration coefficient K (x 10^5) for Unit 16 - Site 1, wind direction 250°, and a wind speed of 3.2 m/s. (1 in = 610 m)

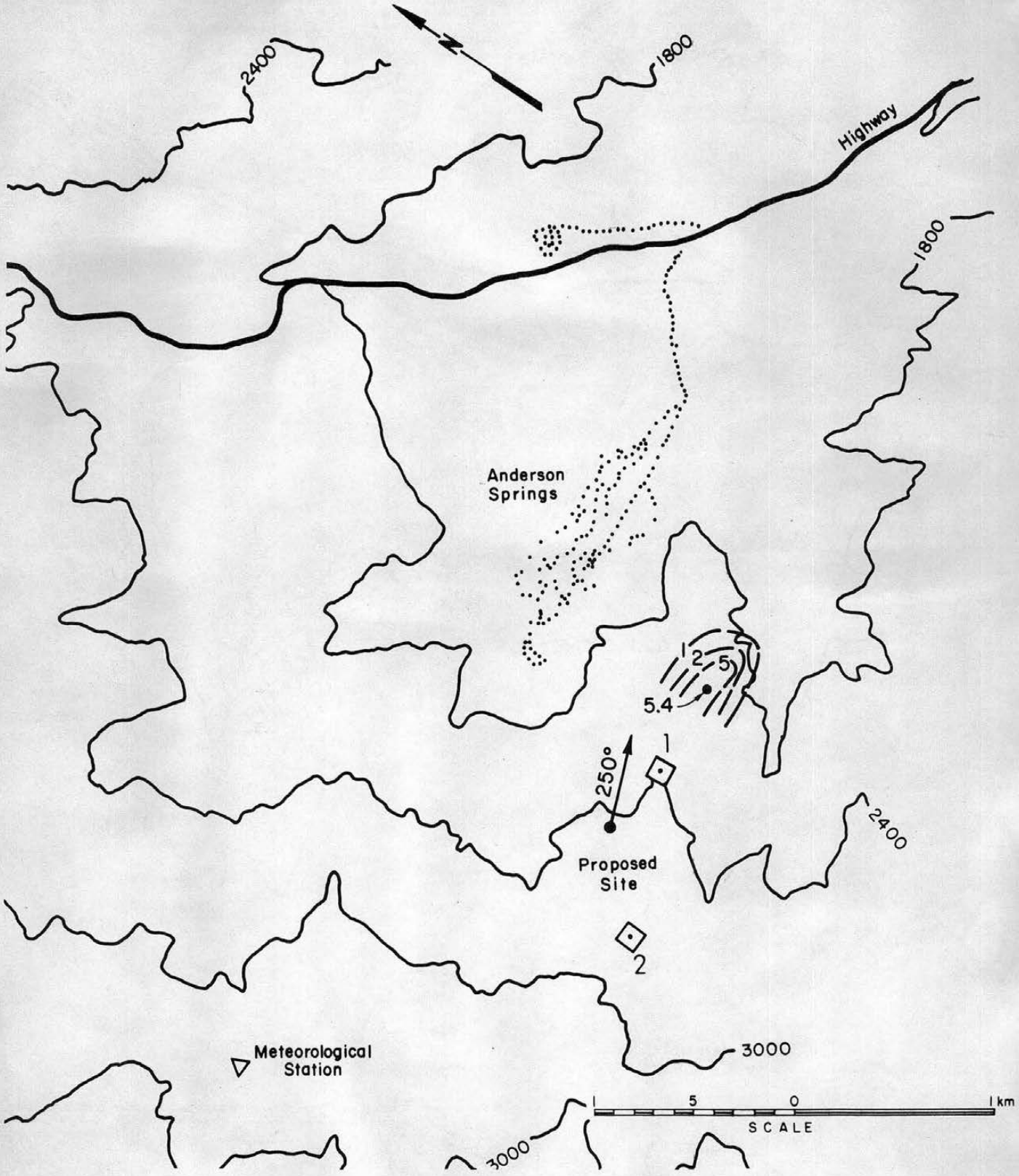

Figure 4.2-8 Isopleths of nondimensional concentration coefficient K (x 10^5) for Unit 16 - Site 1, wind direction 250°, and a wind speed of 6.5 m/s. (1 in = 610 m)

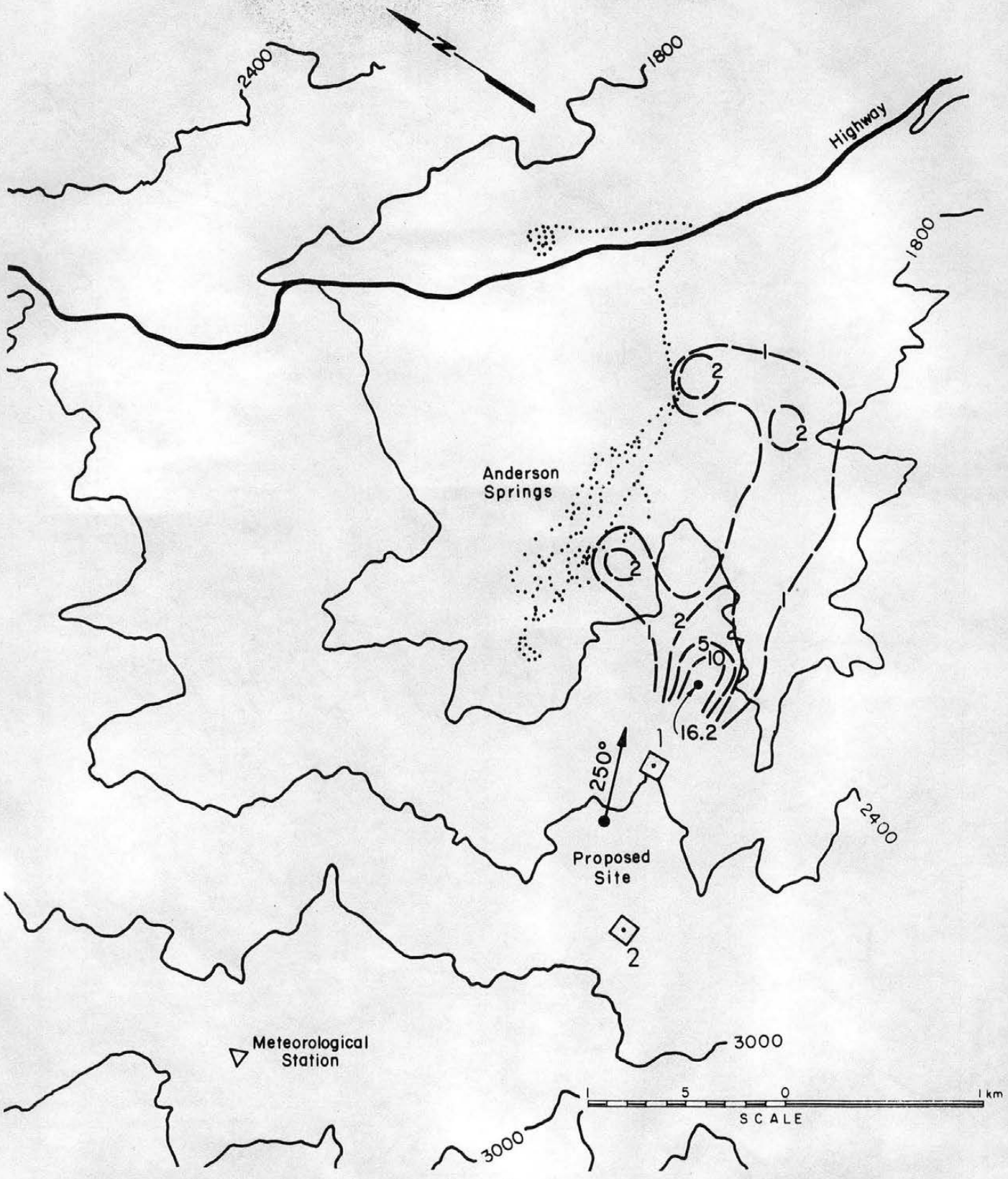

Figure 4.2-9 Isopleths of nondimensional concentration coefficient K (x 10^5) for Unit 16 - Site 1, wind direction 250°, and a wind speed of 9.8 m/s. (1 in = 610 m)

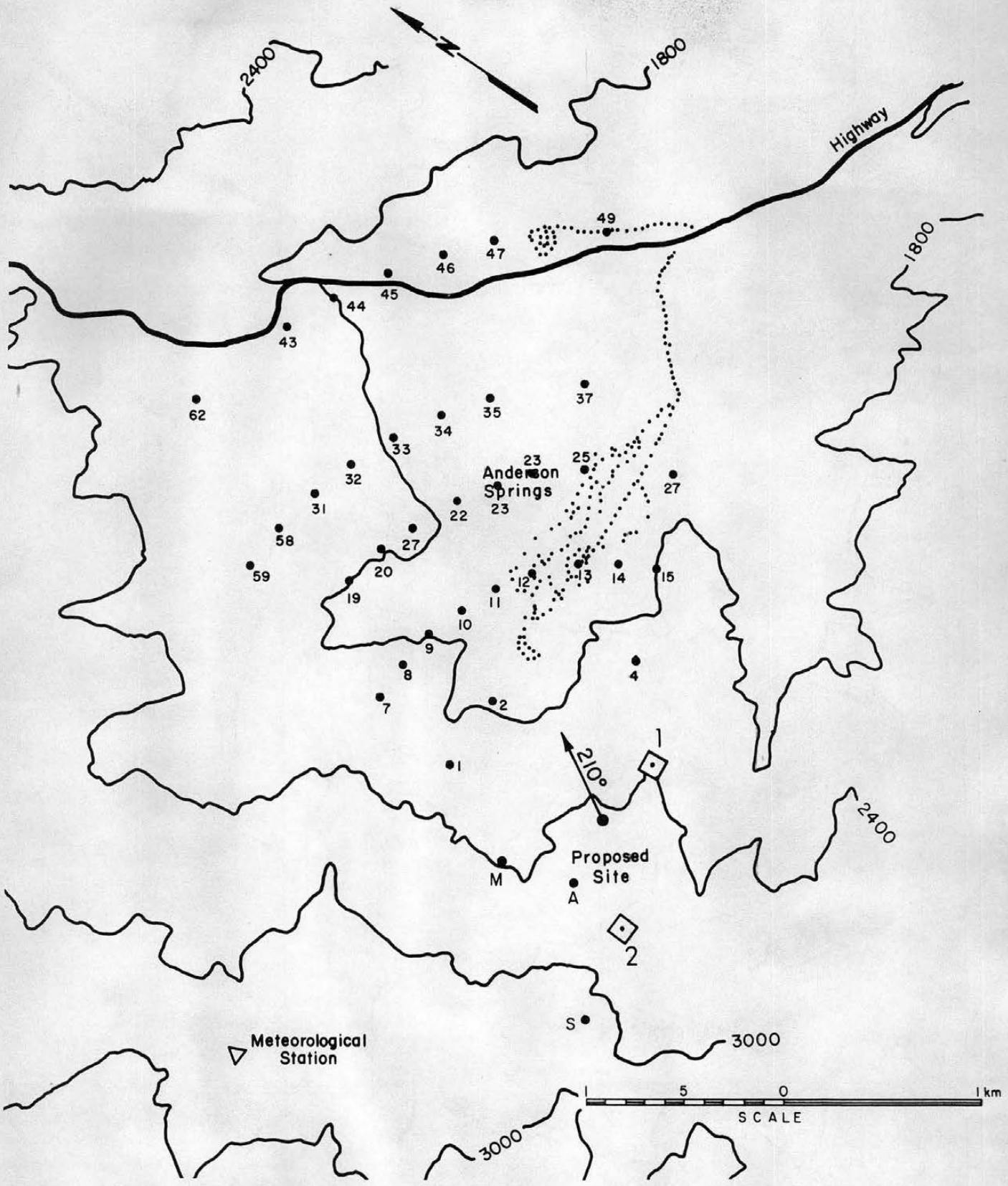

Figure 4.2-10 Base map for wind direction 210°.

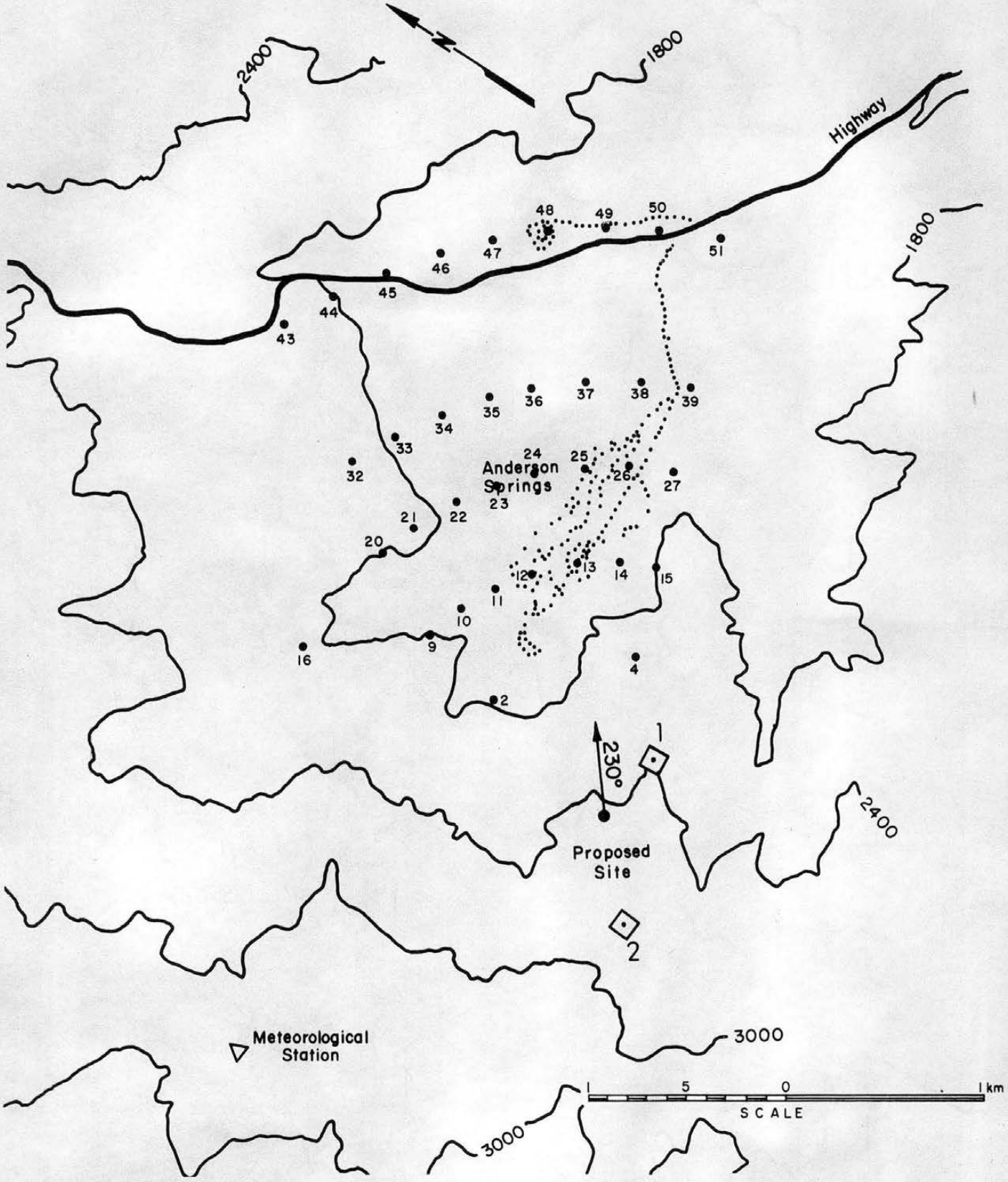

Figure 4.2-11 Base map for wind direction 230°.

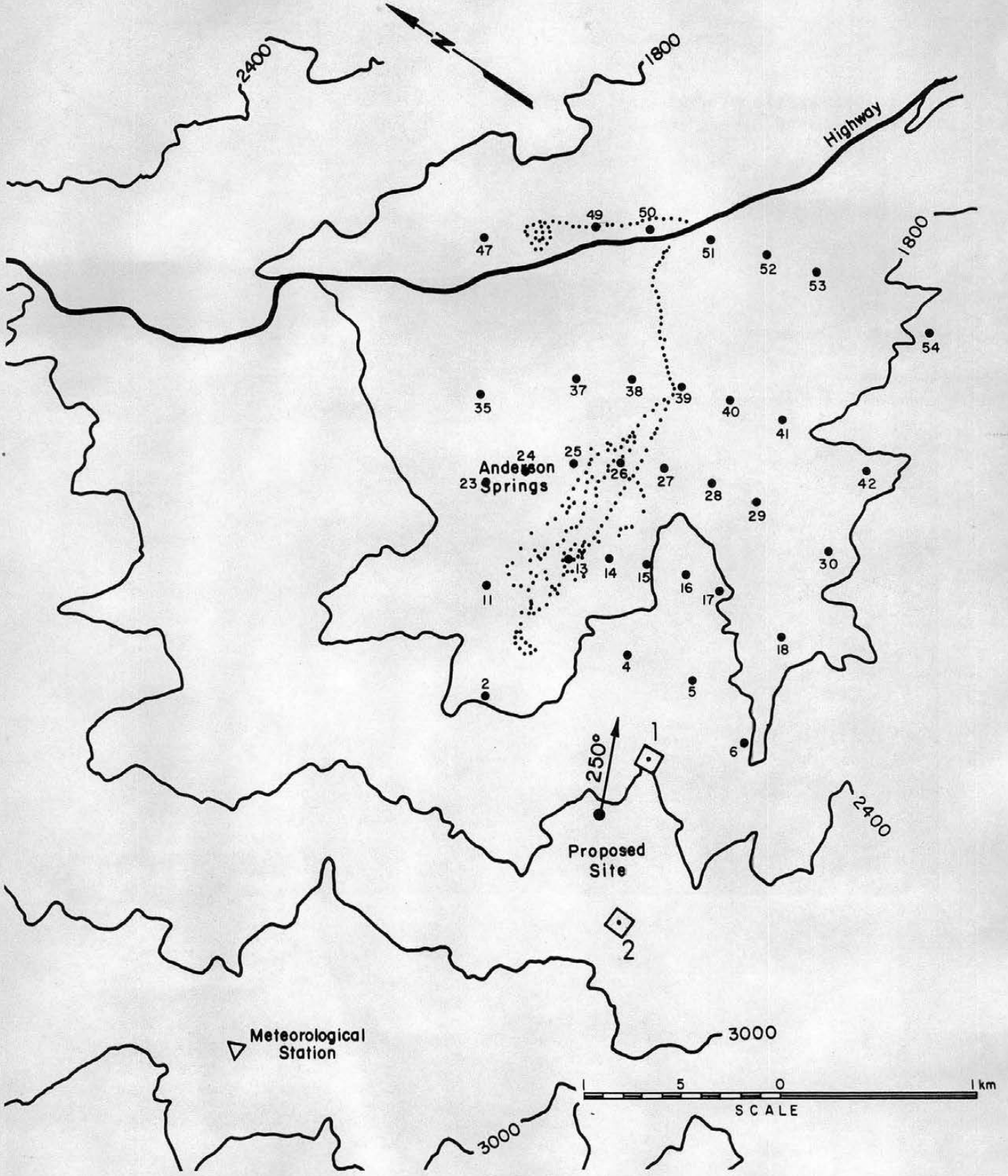

Figure 4.2-12 Base map for wind direction 250°.

Figure 5.1-1

Plume visualization for Unit 16 - Site #2 for Wind Direction 250° and a Wind Speed of

a) 3.2 m/s →

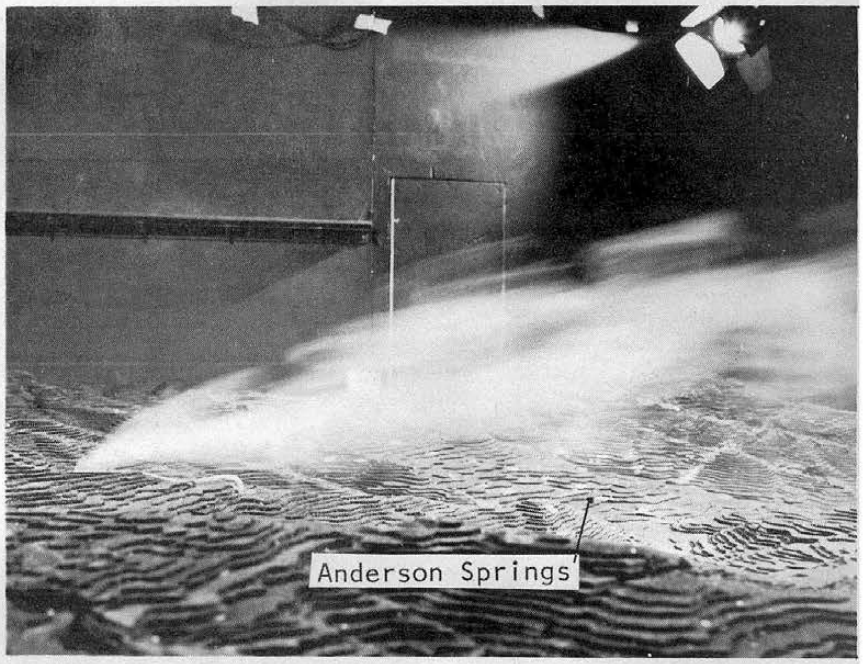

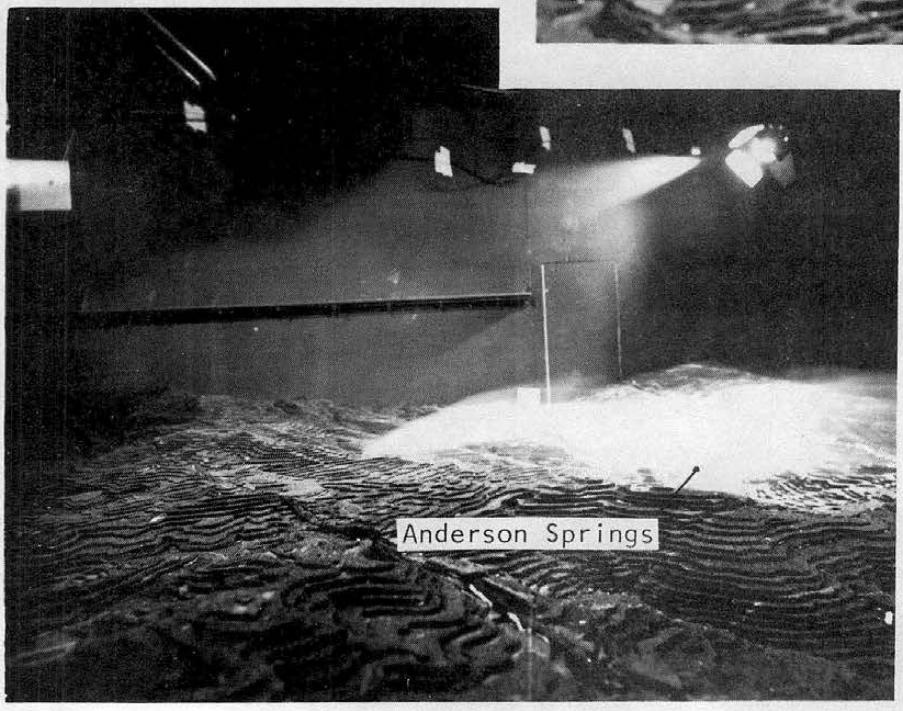

← b) 6.5 m/s

c) 9.8 m/s →

Figure 5.1-2

Plume visualization for Unit 16 - Site #2 for Wind Direction 230° and a Wind Speed of

a) 3.2 m/s →

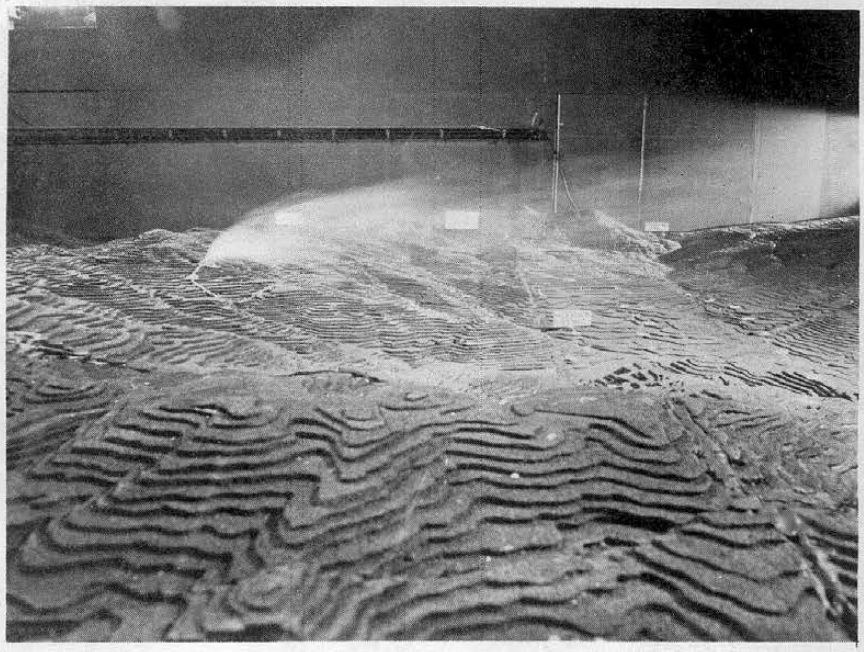

← b) 6.5 m/s

c) 9.8 m/s →

Figure 5.1-3

Plume visualization for Unit 16 - Site #2 for Wind Direction 210° and a Wind Speed of

a) 3.2 m/s →

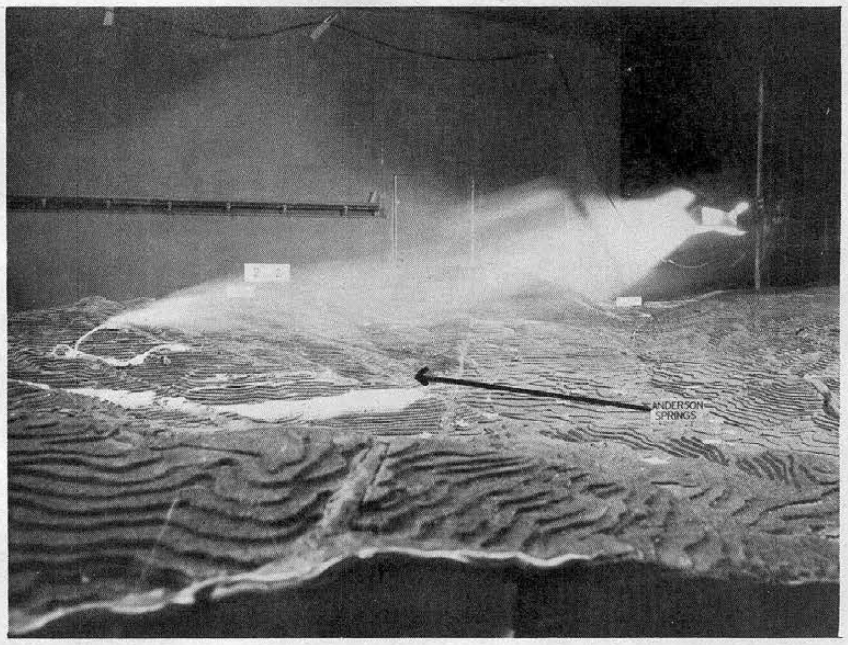

← b) 6.5 m/s

c) 9.8 m/s →

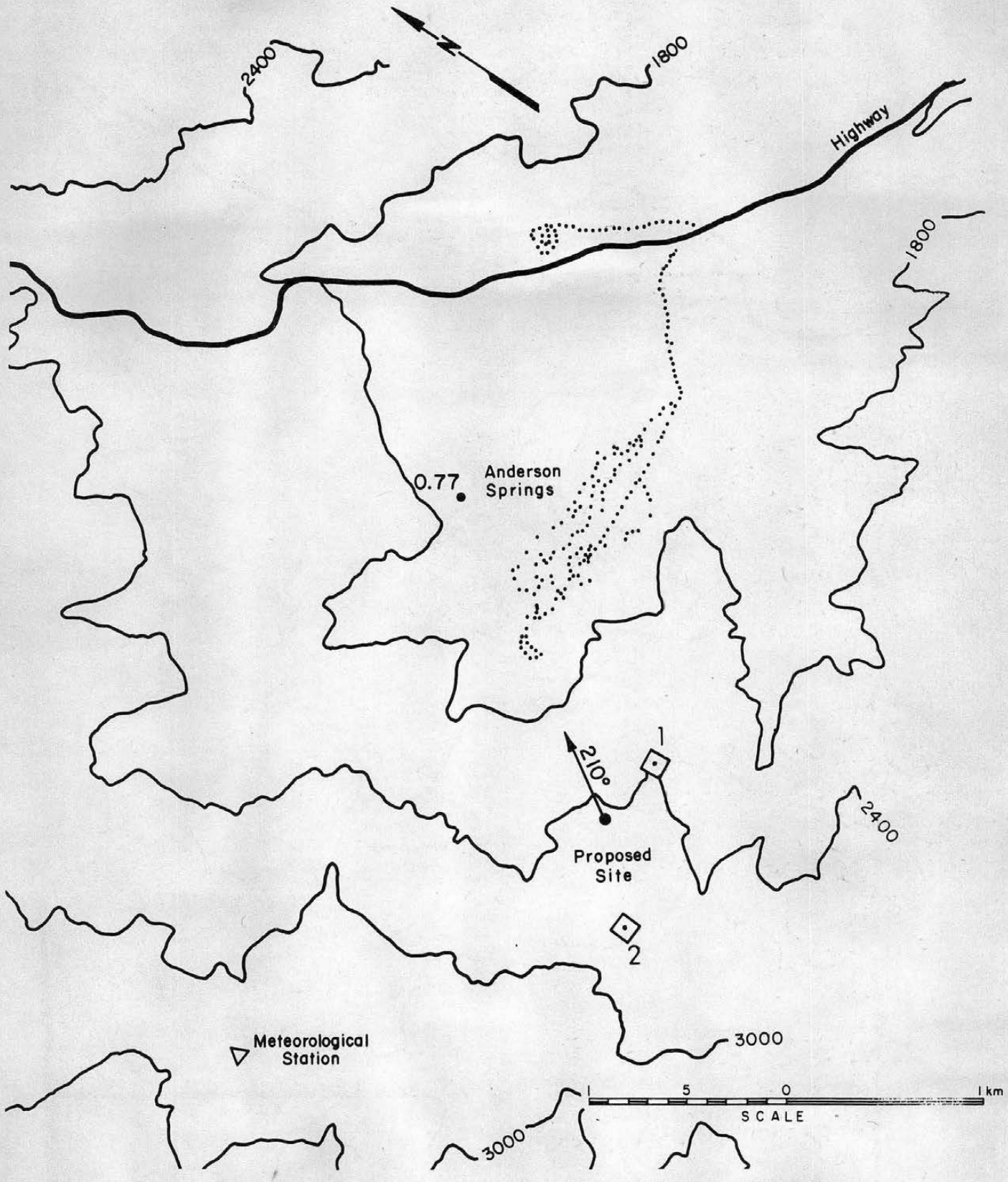

Figure 5.2-1 Isopleths of nondimensional concentration coefficient K (x 10^5) for Unit 16 - Site 2, wind direction 210°, and a wind speed of 3.2 m/s. (1 in = 610 m)

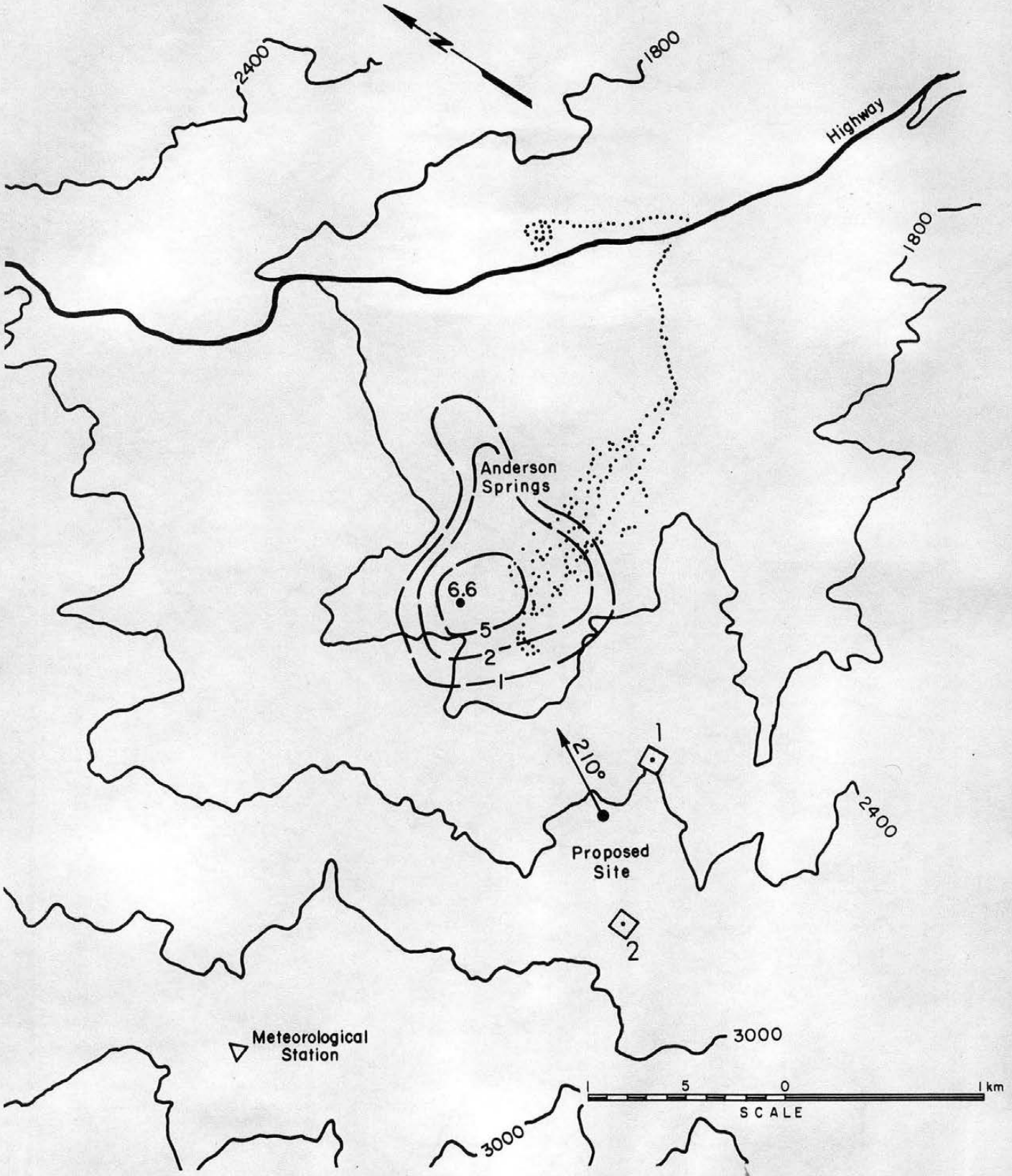

Figure 5.2-2 Isopleths of nondimensional concentration coefficient K (x 10^5) for Unit 16 - Site 2, wind direction 210°, and a wind speed of 6.5 m/s. (1 in = 610 m)

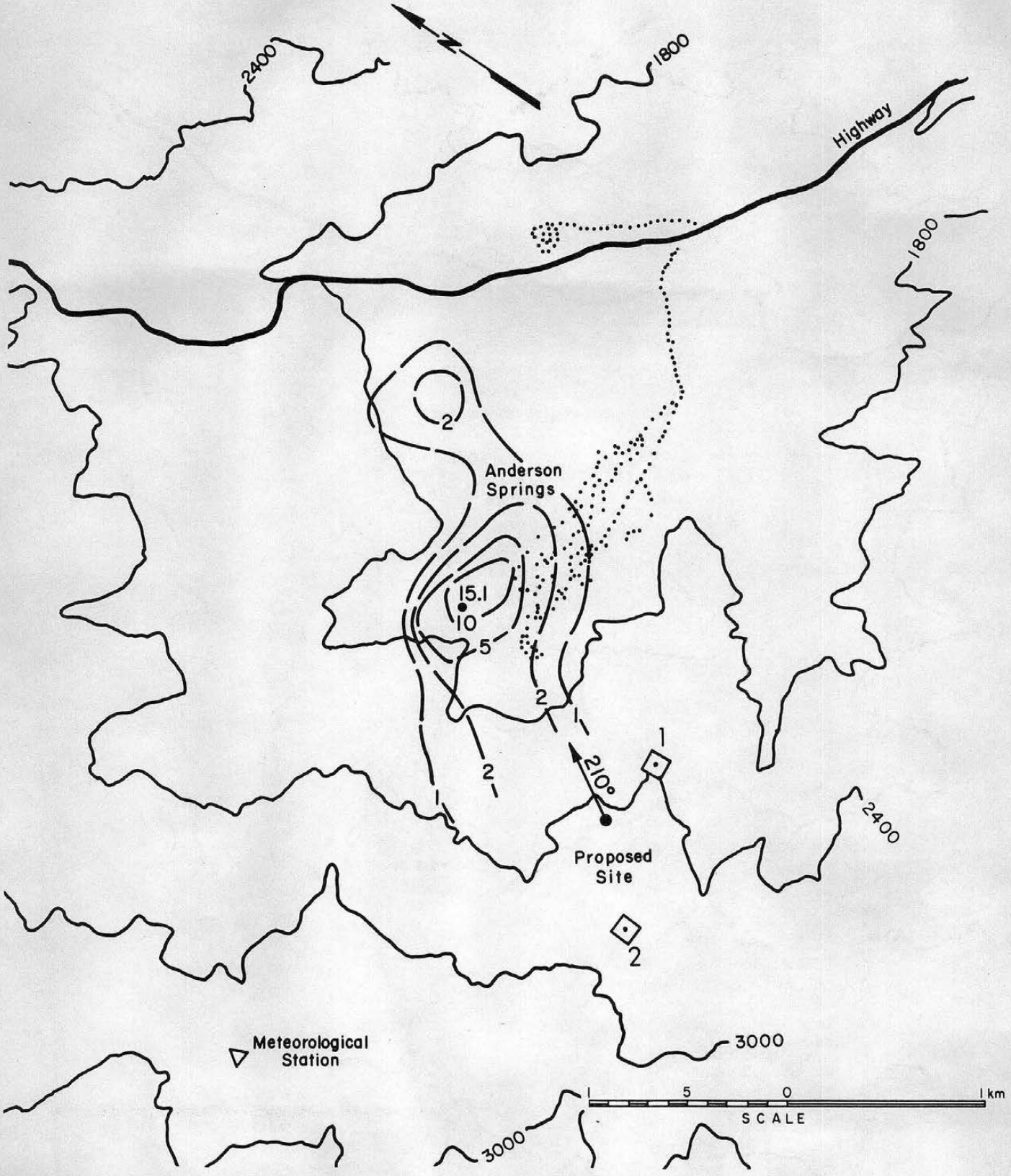

Figure 5.2-3 Isopleths of nondimensional concentration coefficient K (x 10^5) for Unit 16 - Site 2, wind direction 210°, and a wind speed of 9.8 m/s. (1 in = 610 m)

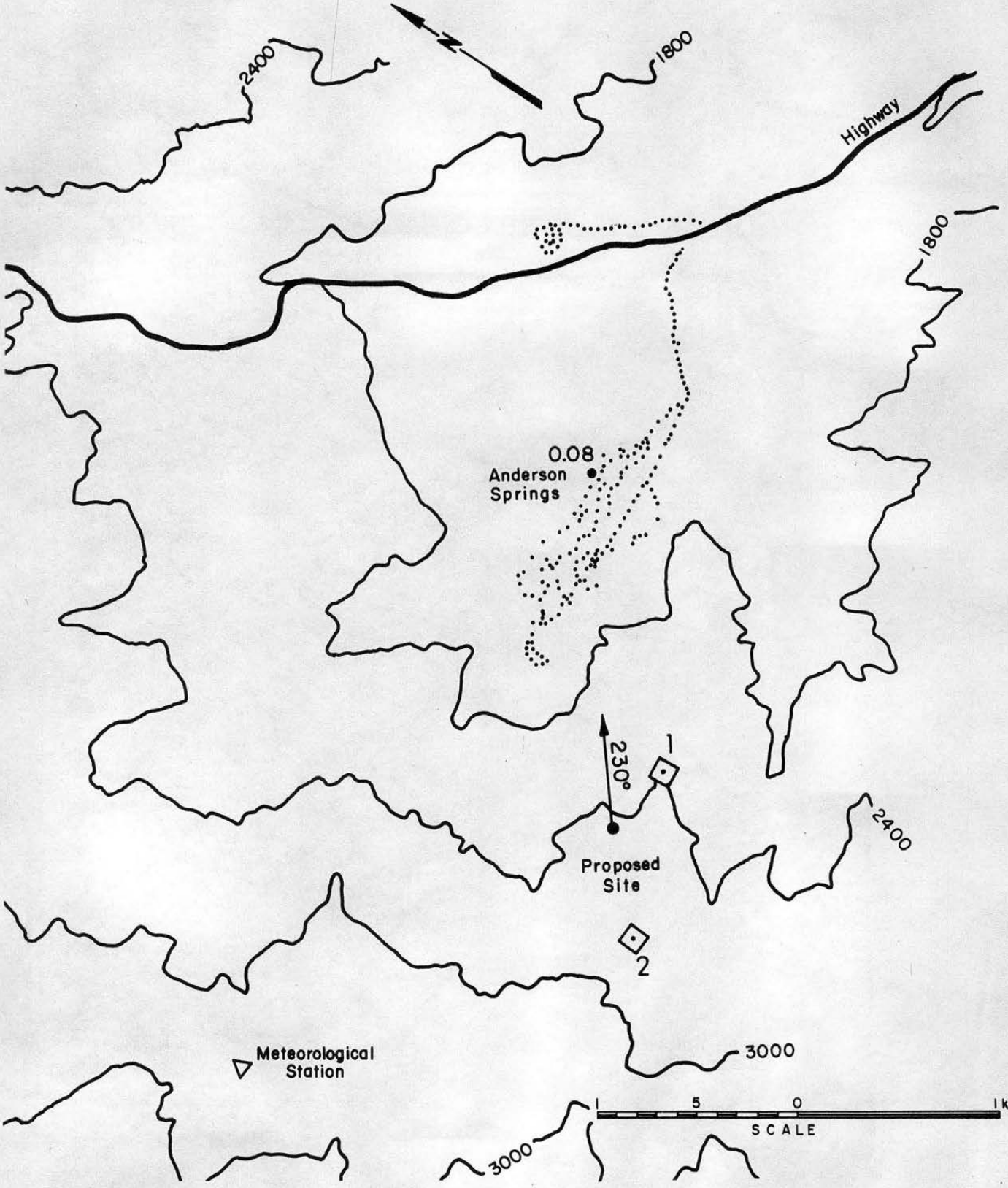

Figure 5.2-4 Isopleths of nondimensional concentration coefficient K ($\times 10^5$) for Unit 16 - Site 2, wind direction 230°, and a wind speed of 3.2 m/s. (1 in = 610 m)

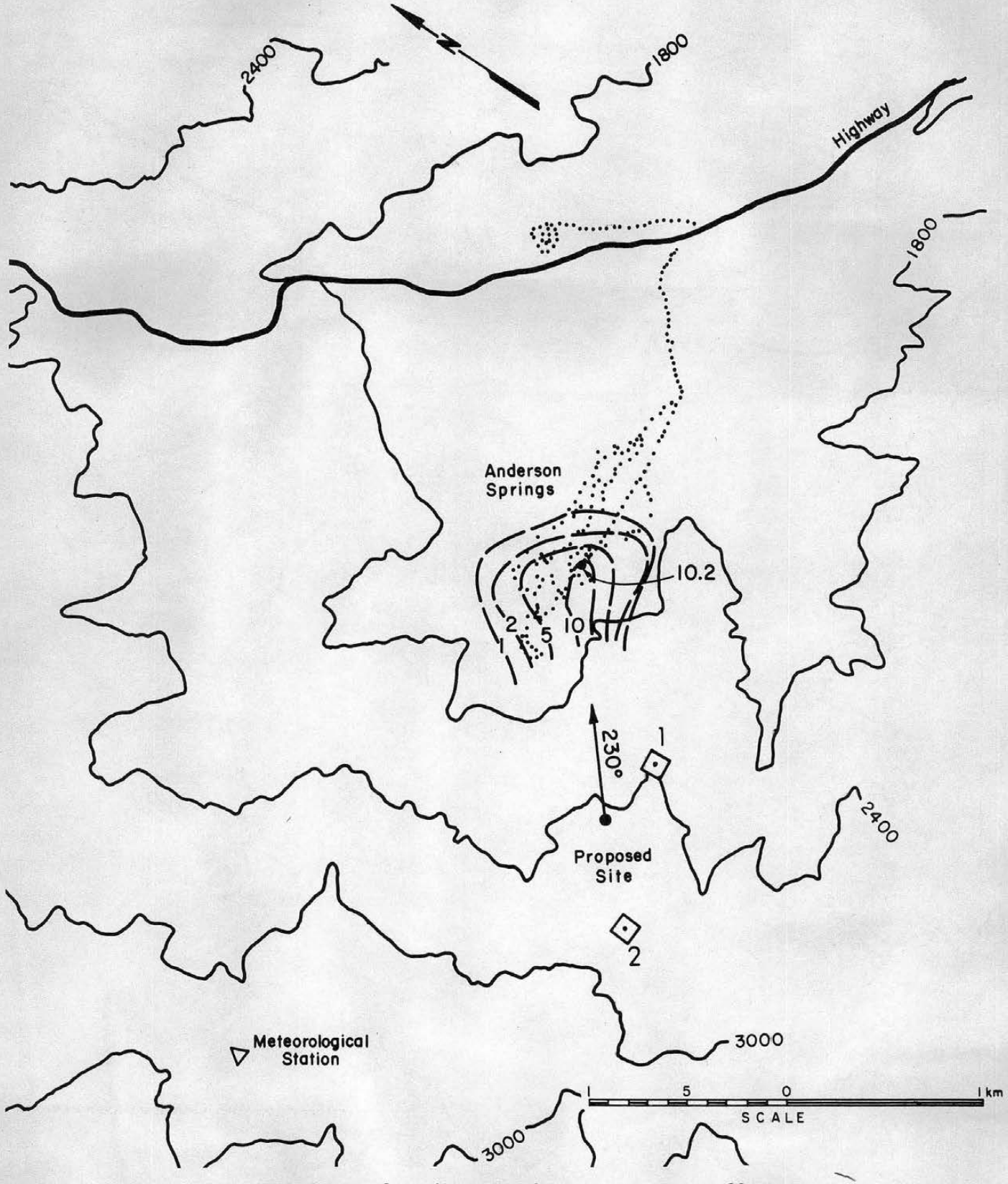

Figure 5.2-5 Isopleths of nondimensional concentration coefficient K (x 10^5) for Unit 16 - Site 2, wind direction 230°, and a wind speed of 6.5 m/s. (1 in = 610 m)

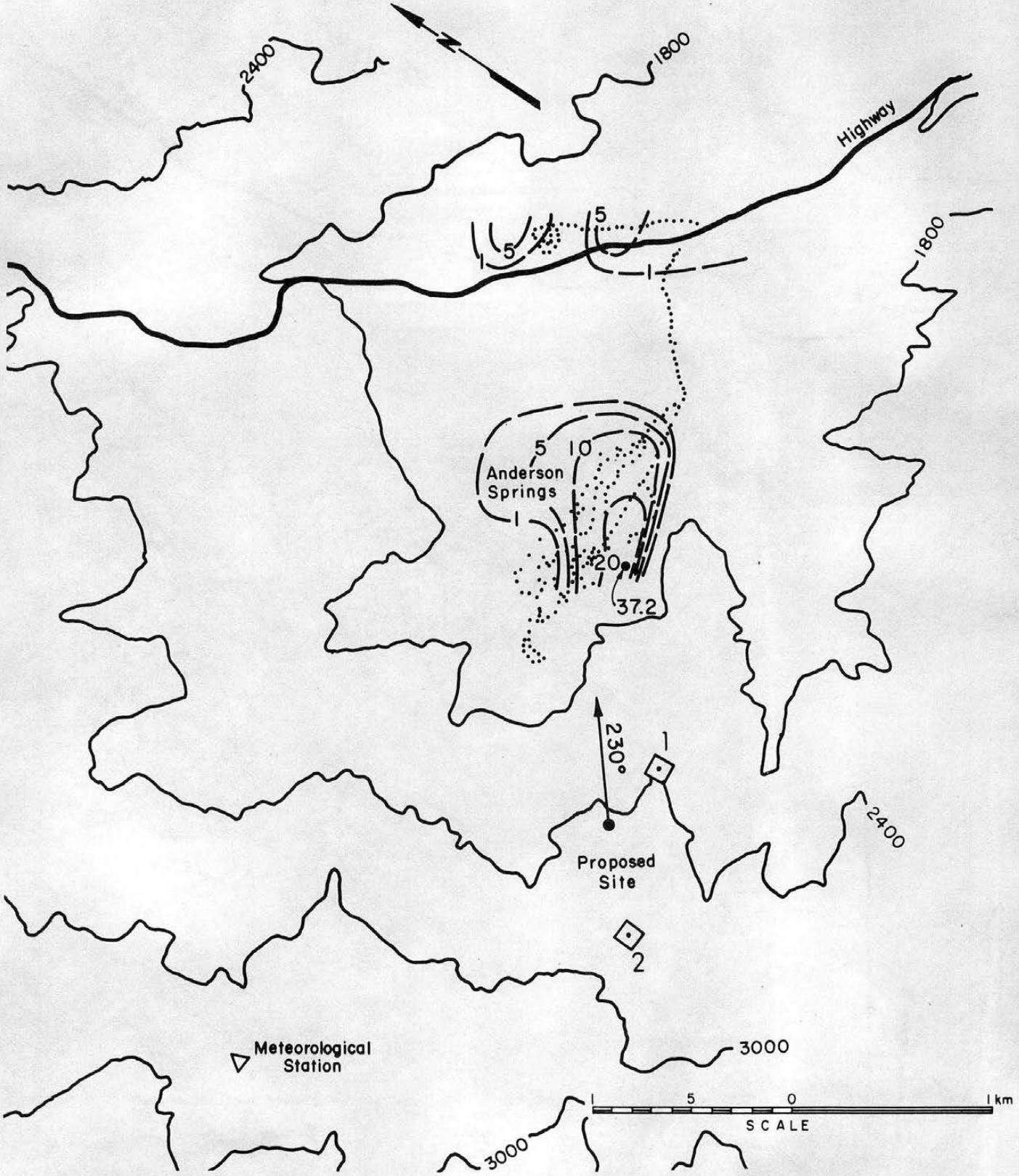

Figure 5.2-6 Isopleths of nondimensional concentration coefficient K (x 10^5) for Unit 16 - Site 2, wind direction 230°, and a wind speed of 9.8 m/s. (1 in = 610 m)

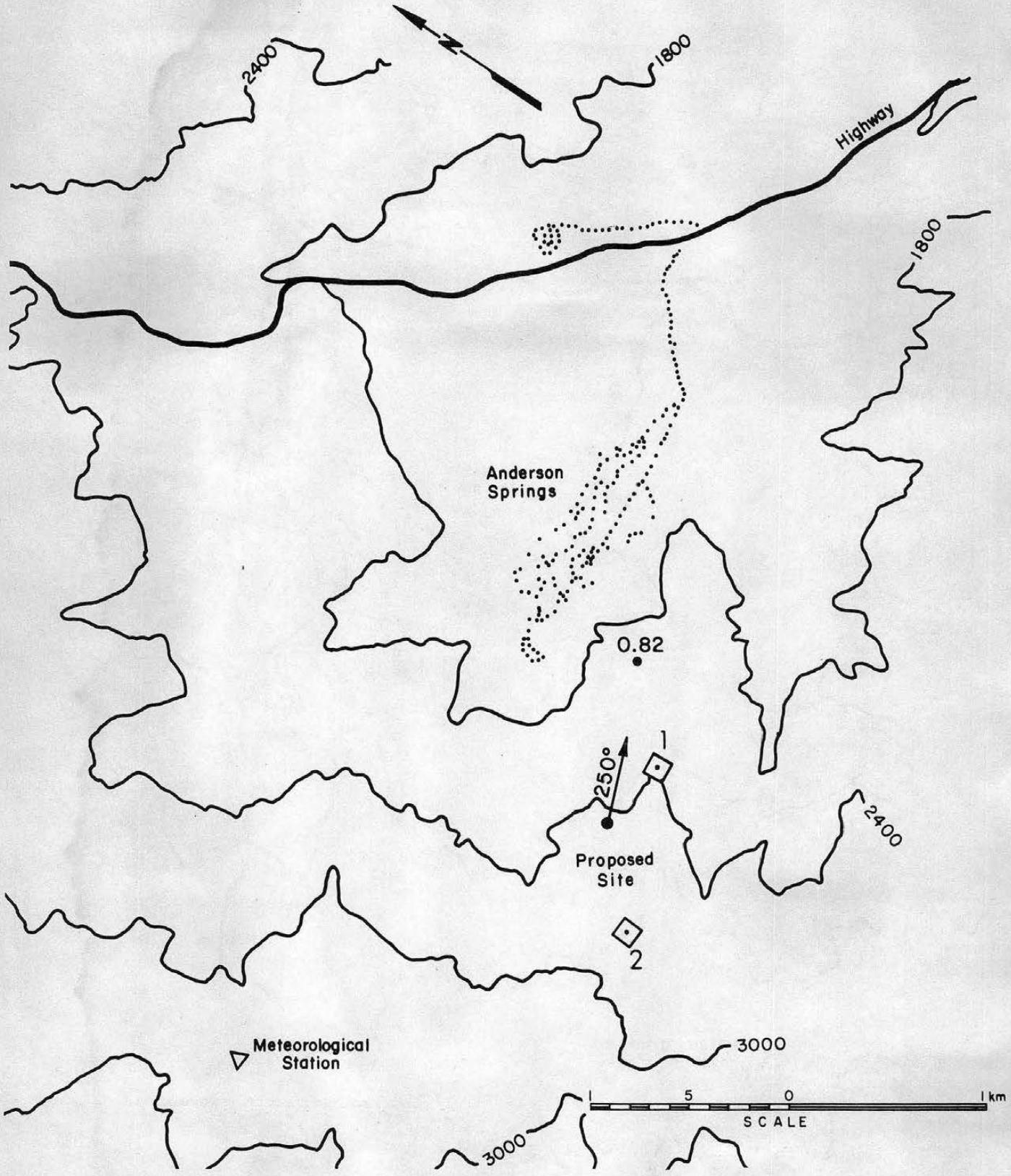

Figure 5.2-7 Isopleths of nondimensional concentration coefficient K (x 10^5) for Unit 16 - Site 2, wind direction 250°, and a wind speed of 3.2 m/s. (1 in = 610 m)

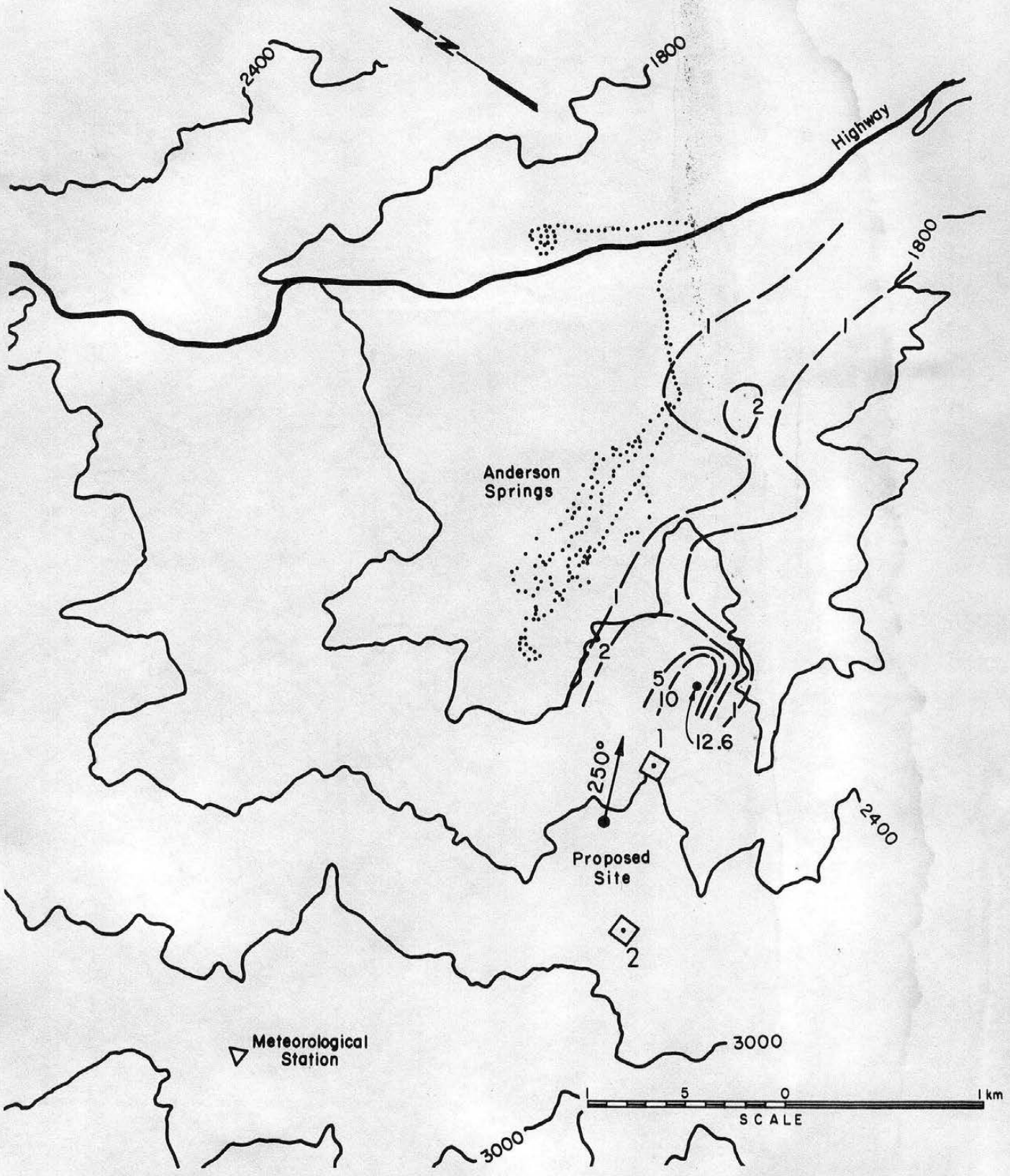

Figure 5.2-8 Isopleths of nondimensional concentration coefficient K (x 10^5) for Unit 16 - Site 2, wind direction 250°, and a wind speed of 6.5 m/s. (1 in = 610 m)

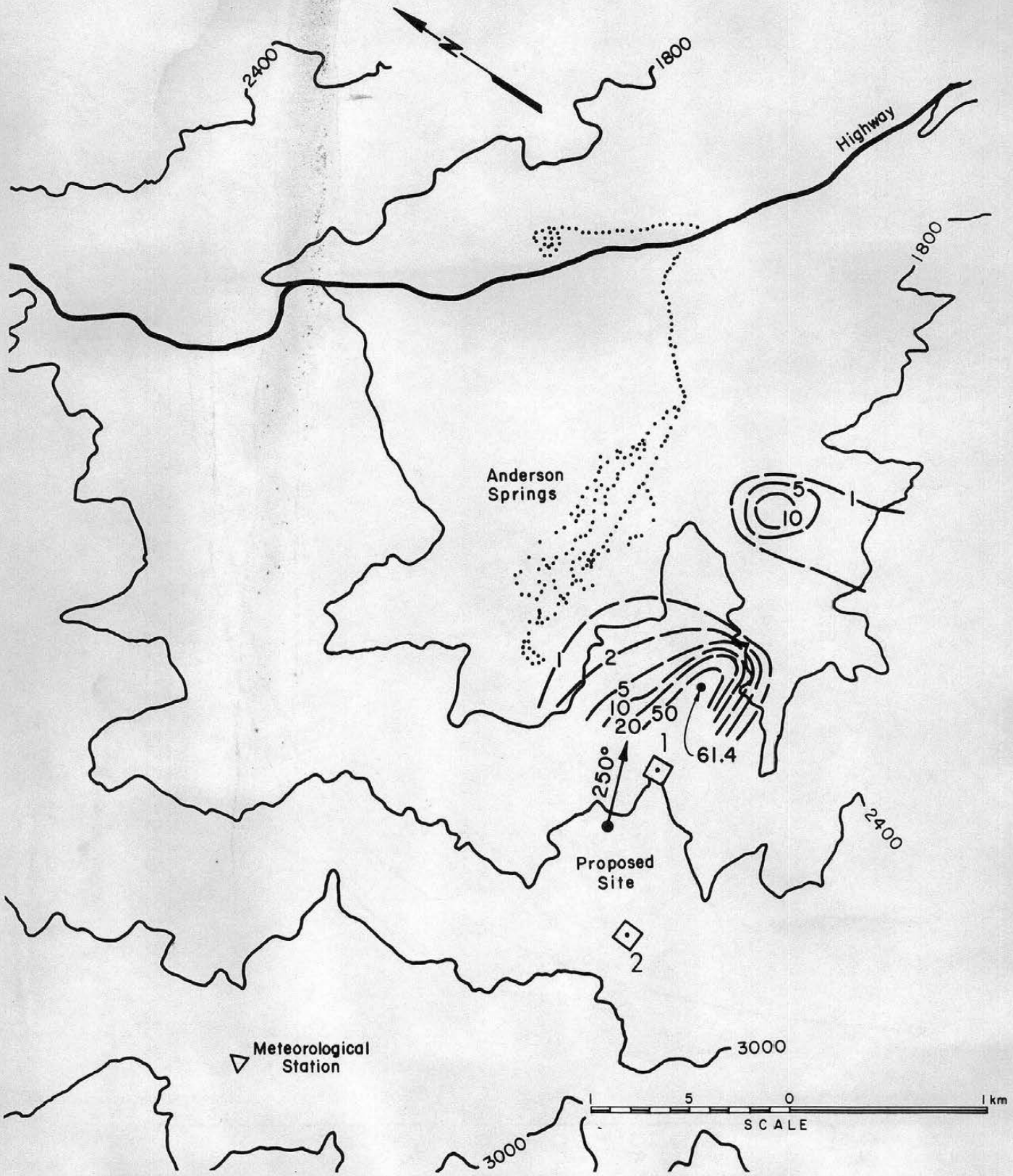

Figure 5.2-9 Isopleths of nondimensional concentration coefficient K (x 10^5) for Unit 16 - Site 2, wind direction 250°, and a wind speed of 9.8 m/s. (1 in = 610 m)

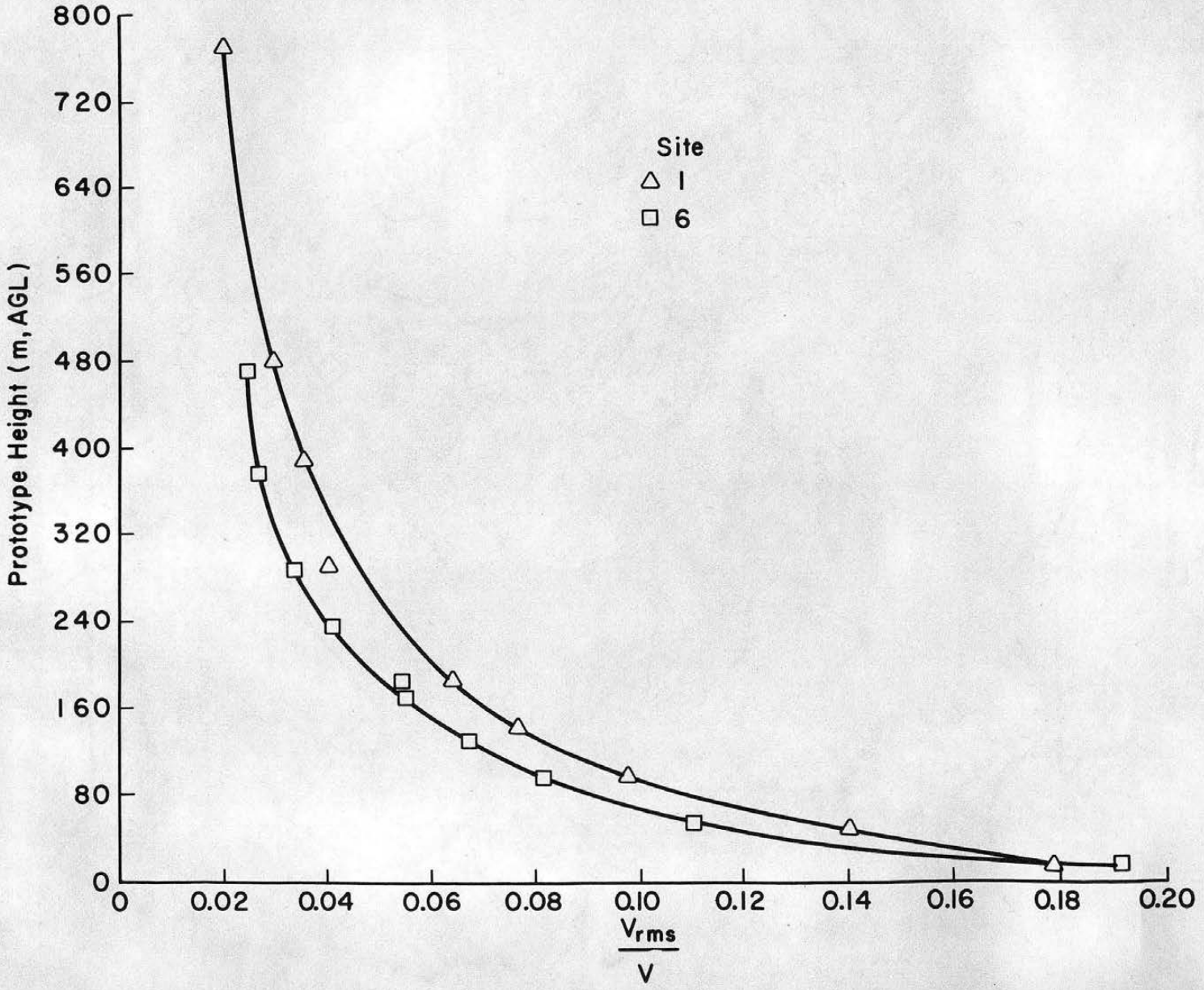

Figure 6-1 Turbulent intensity at Sites 1 and 6.

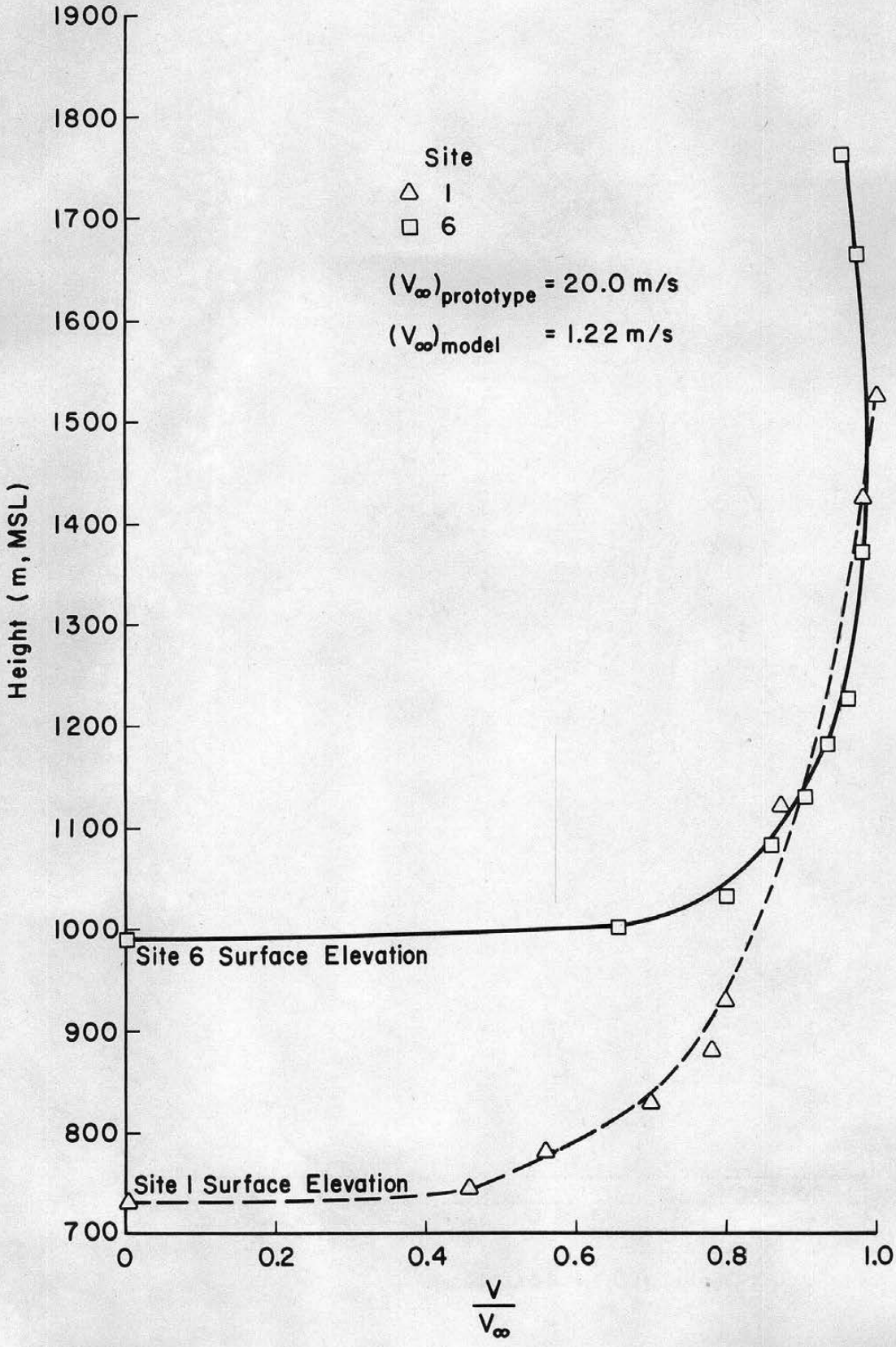

Figure 6-2 Comparison of mean wind tunnel velocity profiles at Sites 1 and 6.

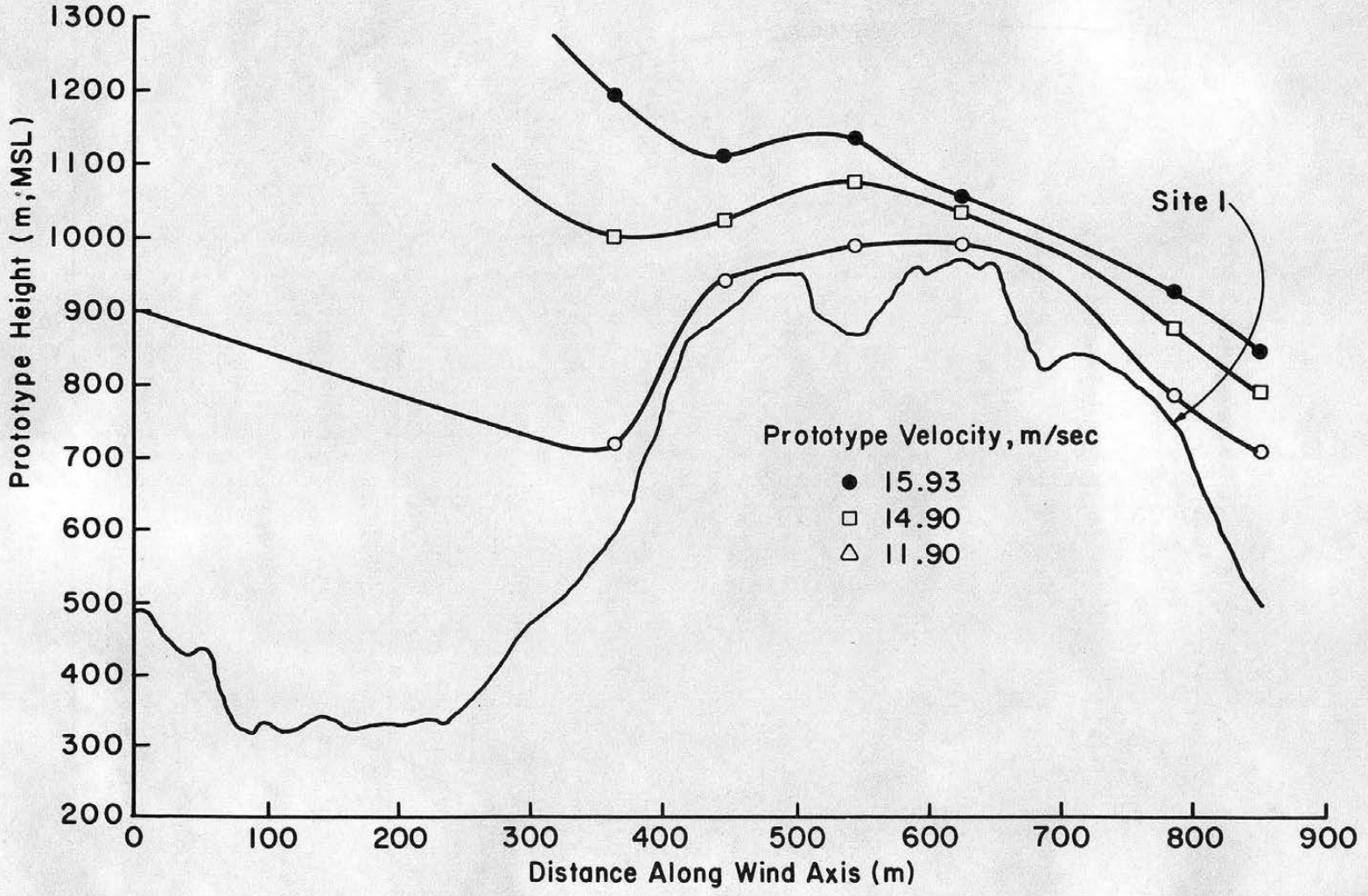

Figure 6-3 Constant velocity lines over the terrain.

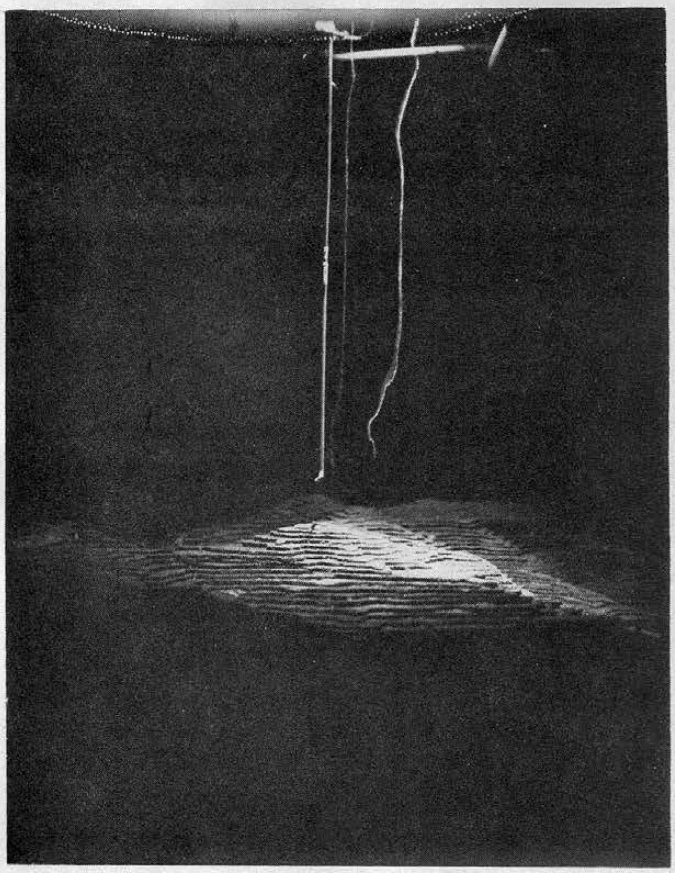

Figure 6-4 Smoke Wire Velocity Profiles
(0.5 second intervals)
taken at three terrain heights near Sites 1 & 2 (Probe height is 1268 m - prototype)

a) 975 m, MSL (Location S)* →

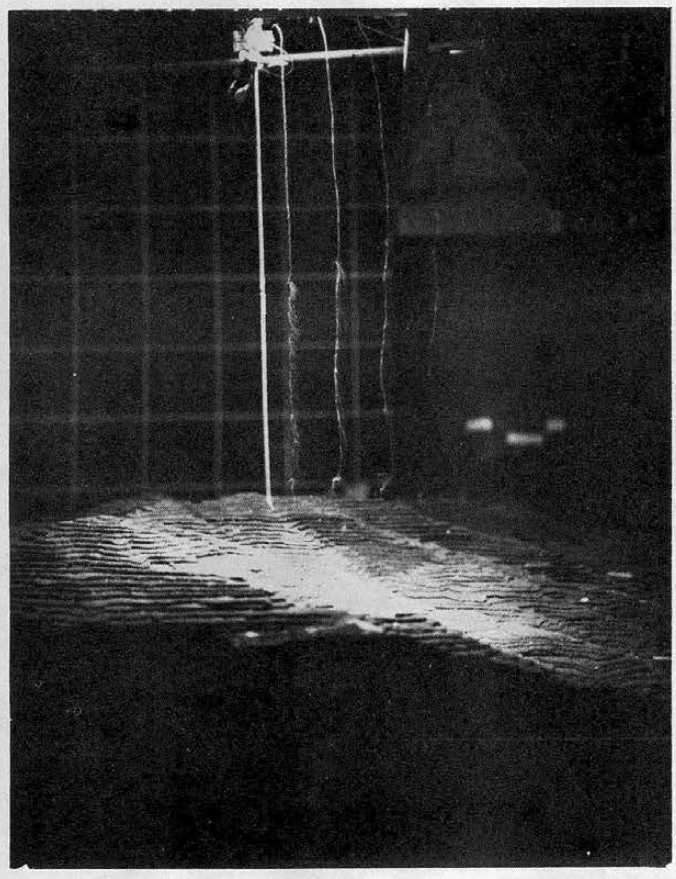

b) 792 m, MSL (Location A)*

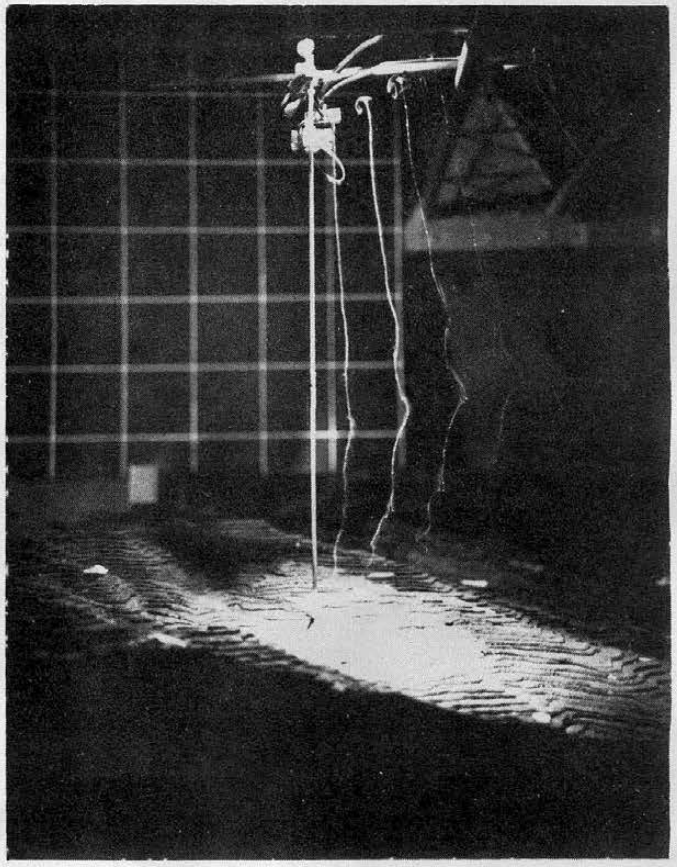

c) 719 m (Location M)* →

*See Figure 4.2-10 for Locations

APPENDIX C

Table 2.1 Model and Prototype Dimensional Parameter for Unit 16 - Sites 1 and 2

Parameter	Prototype	Model
1. Building		
a. length (ℓ)	98m	5.1cm
b. width (w)	21.5m	1.1cm
c. height (h)	20m	1.0cm
2. Exit Temperature (T_s)	319°K	293°K
3. Cell Diameter (D)	9.5m	0.44cm
4. Number of Cells	10	10
5. Exit Velocity (V_s)	7.6 m/s	0.46 m/s
6. Volumetric Emission Rate (Λ)	4312.6 m^3/s @ 319°K & 1 atm	71.32 cc/s @ 293° K & 1 atm
7. Gas Density (ρ_s)	1.07 kg/m^3 @ 319°K & 1 atm	0.29 kg/m^3 @ 293°K & 1 atm
8. Ambient Density (ρ_a)	1.20 kg/m^3 @ 293°K & 1 atm	0.29 kg/m^3 @ 293°K & 1 atm
9. Wind Speed at Meteorological Tower (V_a)	3.2, 6.5, 9.8 m/s	0.20, 0.40, 0.60 m/s
10. Ridge Height above Cooling Tower Elevation (H)	244 m	0.13 m
11. Wind Direction	210°, 230°, and 250° azimuth	
12. Surface Roughness (z_o)	0.5 m	0.02 cm
13. Reference Elevation	1854 m, MSL	46 cm, AGL
14. Reference Velocity ($V\infty$)	5.6, 11.3, 16.8 m/s	0.34, 0.69, 1.03 m/s

Table 2.2 Model and Prototype Dimensionless Parameters for Unit 16 - Sites 1 and 2

Parameter	Prototype	Model
$\frac{\delta_a}{H}$	1.84	2.15
$\frac{z_o}{H}$	2.0×10^{-3}	1.5×10^{-3}
$\frac{D}{H}$	3.5×10^{-2}	3.5×10^{-2}
$\frac{h}{H}$	1.6×10^{-2}	1.6×10^{-2}
$R = \frac{V_s}{V_a}$	1.7, .85, .57	1.7, .84, .56
$Fr = \frac{\rho_a V_a^2}{g(\rho_a - \rho_s)D}$	1.1, 4.6, 10.5	1.1, 4.6, 10.5
$DR = \frac{\rho_a - \rho_s}{\rho_a}$	.11	.79
$Re_{L_o} = \frac{V_\infty \rho_a L_o}{\mu_a}$	1.0×10^{10} 2.0×10^{10} 3.0×10^{10}	3.1×10^{5} 6.2×10^{5} 9.3×10^{5}
$R_o = \frac{V_\infty}{H\Omega}$	229, 459, 689	26154, 53077, 79231

Table 3.5-1 Hot Wire Calibration

LEAST SQUARES CURVE FIT - HOT WIRE CALIBRATION DATA- E**2/R(R-RA)=A+B*U**C

HOT WIRE CALIBERATION (8583), JAN. 31 SAMIR

13 DATA POINTS. HOT RESISTANCE= 8.175 COLD RESISTANCE= 5.450

FIRST ESTIMATE FOR EXPONENT C = .600

U(DATA)	E(DATA)	SOLUTIONS-	U**C	E**2/R(R-RA)	E
.3525	2.52100		.4976	.28515	2.52039
.4430	2.53400		.5798	.28816	2.53363
.5209	2.54400		.6462	.29059	2.54429
.7421	2.57100		.8190	.29691	2.57181
.8727	2.58600		.9128	.30034	2.58663
.9895	2.59900		.9930	.30327	2.59922
1.0965	2.61000		1.0636	.30586	2.61027
1.2025	2.62100		1.1314	.30833	2.62082
1.3019	2.63100		1.1932	.31059	2.63041
2.1367	2.70300		1.6624	.32776	2.70211
2.9700	2.76300		2.0725	.34275	2.76323
3.8762	2.82200		2.4769	.35754	2.82222
4.5944	2.86500		2.7754	.36846	2.86499

CONVERGENCE WAS SUCCESSFUL AFTER 4 ITERATIONS

LEAST SQUARES EQUATION IS E**2/R(R-RA)= .2669551 + .0365732 U** .6694

FOR EACH ITERATION, VALUES ARE

C	DELTA C	A	B	SUM SQ
.6000	.12120	.2614048	.0425116	.449349E-05
.6500	.02188	.2655217	.0381117	.500098E-06
.6719	-.00244	.2671287	.0363866	.173776E-06
.6694	-.00003	.2669551	.0365732	.168454E-06

Table 4.1-1 Summary of Photographs Taken
For Unit 16 - Site 1

Photo or Run #	Wind Direction	Wind Speed (m/s)
1	250°	4.5
4	250°	8.9
7	250°	13.4
10	230°	4.5
13	230°	8.9
16	230°	13.4
19	210°	4.5
20	210°	8.9
21	210°	13.4

Table 4.2-1 NONDIMENSIONAL CONCENTRATION COEFFICIENTS ($\times 10^5$)
FOR UNIT 16 - SITE 1
AND A WIND DIRECTION OF 210°

	Wind Speed (ms^{-1})		
Location Number	3.2	6.5	9.8
1	0.41	0.54	1.08
2	0.85	1.71	5.28
4	6.61	25.94	90.75
7	0.00	0.08	0.13
8	0.01	0.08	0.02
9	0.00	0.02	0.04
10	0.00	0.06	0.07
11	0.00	0.42	1.10
12	0.19	4.48	14.92
13	1.62	15.58	53.01
14	0.07	5.81	7.65
15	0.00	0.10	0.43
19	0.01	0.05	0.04
21	0.00	0.01	0.00
22	0.00	0.02	0.36
23	0.19	4.83	22.83
24	0.08	0.03	0.17
25	0.00	0.00	0.05
27	0.01	0.01	0.10
59	0.01	0.00	0.04
58	0.00	0.02	0.08
31	0.01	0.03	0.10
32	0.00	0.01	0.05
33	0.03	0.31	0.70
34	2.67	1.69	2.01
35	0.02	0.06	0.14
37	0.01	0.03	0.07
62	0.10	0.10	0.21
43	0.01	0.03	0.17
44	0.00	0.05	0.28
45	0.00	0.02	0.16
46	0.04	0.78	17.00
47	0.08	0.24	0.44
49	0.04	0.25	0.41

Table 4.2-2 NONDIMENSIONAL CONCENTRATION COEFFICIENTS ($\times 10^5$)
FOR UNIT 16 - SITE 1
AND A WIND DIRECTION OF 230°

	Wind Speed (ms^{-1})		
Location Number	3.2	6.5	9.8
2	0.06	0.01	0.06
4	0.21	5.19	21.02
9	0.00	0.01	0.01
10	0.02	0.03	0.02
11	0.01	0.02	0.03
12	0.02	0.01	0.00
13	0.01	0.00	0.13
14	0.06	1.69	12.61
15	0.48	5.05	30.59
20	0.01	0.07	0.47
21	0.02	0.07	0.06
22	0.01	0.01	0.03
23	0.01	0.02	0.10
24	0.02	0.00	0.06
25	0.02	0.05	0.14
26	0.11	0.90	1.36
27	0.86	0.04	0.46
32	0.02	0.03	0.29
33	0.04	0.06	0.31
34	0.04	0.03	0.07
35	0.02	0.02	0.22
36	0.05	0.03	0.21
37	0.05	0.02	0.22
38	0.36	0.00	0.39
39	0.08	0.06	0.06
43	0.03	0.05	0.06
44	0.05	0.04	--
45	0.02	0.04	0.04
46	0.06	0.05	0.15
47	0.04	0.02	0.08
48	0.06	0.06	0.15
49	0.46	1.05	0.34
50	0.99	0.34	0.19
51	0.95	0.34	0.22

Table 4.2-3 NONDIMENSIONAL CONCENTRATION COEFFICIENTS ($\times 10^5$)
FOR UNIT 16 - SITE 1
AND A WIND DIRECTION OF 250°

	Wind Speed (ms^{-1})		
Location Number	3.2	6.5	9.8
2	0.08	0.06	0.67
4	1.63	0.00	0.17
5	1.05	5.43	16.17
6	0.25	0.17	0.40
11	--	0.17	0.36
13	0.06	0.11	0.48
14	2.33	0.06	2.38
15	0.01	0.21	1.04
16	0.06	0.07	0.40
17	0.12	0.15	3.50
18	0.31	0.06	0.25
23	0.15	0.15	0.62
24	0.10	0.06	0.08
25	0.09	0.13	0.08
26	0.06	0.07	0.11
27	0.13	0.17	0.17
28	0.00	0.07	0.22
29	0.00	0.77	1.88
30	0.47	0.07	0.00
35	0.64	0.19	0.11
37	0.69	0.19	0.03
38	0.05	0.20	0.08
39	0.08	0.67	3.14
40	0.00	0.73	1.00
41	0.64	0.28	2.80
42	9.15	0.32	0.48
47	0.18	0.12	0.34
49	0.13	0.20	0.48
50	0.45	0.22	0.34
51	0.27	0.07	0.31
52	--	0.17	0.22
53	1.52	0.13	0.73
54	0.12	0.10	0.22

Table 4.2-4 Prototype Sampling Location Key* and Site Location Key

Location #	x (m)	y (m)	z (m, MSL)	Location #	x (m)	y (m)	z (m, MSL)
1	-182.88	810.77	597.4	39	2029.97	804.67	402.3
2	195.07	804.67	524.3	40	2103.12	548.64	390.1
3	512.06	640.08	499.9	41	2151.89	292.61	487.7
4	755.09	304.8	609.6	42	2157.98	-201.17	499.9
5	816.86	-30.48	621.8	43	1194.82	2682.24	585.2
6	682.75	420.62	560.8	44	1450.85	2554.	536.4
7	-79.25	1286.26	597.4	45	1694.69	2401.8	499.9
8	109.73	1280.16	548.6	46	1914.14	2218.9	499.9
9	304.8	1255.78	517.44	47	2109.22	2036.1	463.3
10	487.68	1188.72	463.3	48	2304.29	1816.6	426.7
11	664.46	1097.28	451.1	49	2462.78	1591.1	402.3
12	816.86	987.55	426.7	50	2596.9	1353.3	402.3
13	999.74	816.86	438.9	51	2718.82	1060.7	402.3
14	1103.38	646.18	451.1	52	2810.26	780.3	451.1
15	1188.72	475.49	536.4	53	2877.31	530.4	560.8
16	1249.68	280.42	621.8	54	2926.08	-97.5	621.8
17	1280.16	85.34	548.6	56	-97.54	1755.6	597.4
18	1243.58	-298.7	463.3	57	-499.87	1676.4	609.6
19	304.8	1731.26	548.6	58	391.38	2170.2	633.9
20	524.26	1676.4	560.8	59	97.5	2182.4	646.2
21	707.14	1609.34	573	60	-396.2	2158.0	682.8
22	935.74	1493.52	536.4	61	938.8	2779.8	573.0
23	1097.28	137.16	499.9	62	658.4	2865.1	597.4
24	1243.84	1243.58	487.7	63	60.96	2926.1	719.3
25	1402.08	1054.61	426.7	64	670.56	3596.6	670.6
26	1536.19	847.34	390.1	70	-670.56	2072.6	737.6
27	1627.63	646.18	438.9	71	-1798.3	2255.5	722.4
28	1694.69	402.34	438.9	73	-487.68	2804.2	725.4
29	1743.46	170.69	438.9	74	914.4	2804.2	749.8
30	1725.17	-268.22	499.9	75	61.0	4389.1	731.5
31	573.02	2115.31	609.6	76	487.7	4937.8	792.5
32	804.67	2029.97	560.8	77	121.9	3657.6	765.0
33	1024.13	1926.34	524.3	Sites			
34	1243.58	1786.13	512.1	1	402.3	-79.2	719.3
35	1444.75	1633.73	475.5	2	-390.1	-402.3	854.0
36	1597.15	1475.23	463.3	3	-2450.6	182.9	829.1
37	1767.84	1267.97	426.7	Met Station	-2011.7	786.4	1005.8
38	1914.14	1024.13	402.3				

* All locations are with respect to the point represented by the base of the wind direction arrow in Figure 1.1

Table 5.1-1 Summary of Photographs Taken
For Unit 16 - Site 2

Photograph or Run #	Wind Direction	Wind Speed (m/s)
2	250°	4.5
5	250°	8.9
8	250°	13.4
11	230°	4.5
14	230°	8.9
17	230°	13.4
22	210°	4.5
23	210°	8.9
24	210°	13.4

Table 5.2-1 NONDIMENSIONAL CONCENTRATION COEFFICIENTS (x 10^5)
FOR UNIT 16 - SITE 2
AND A WIND DIRECTION OF 210°

	Wind Speed (ms^{-1})		
Location Number	3.2	6.5	9.8
1	0.13	0.22	1.05
2	0.11	0.38	3.77
4	0.02	0.14	0.30
7	0.01	0.02	0.01
8	0.01	0.23	0.61
9	0.10	1.74	6.18
10	0.21	6.63	15.09
11	0.20	5.46	10.57
12	0.18	4.97	3.74
13	0.09	1.99	0.97
14	0.07	0.09	0.54
15	0.00	0.04	0.05
19	0.01	0.05	0.02
21	0.22	0.04	0.10
22	0.77	0.11	0.63
23	0.56	2.40	1.35
24	0.16	0.15	0.89
25	0.00	0.00	0.01
27	0.01	0.02	0.03
59	0.04	0.09	0.00
58	0.06	0.20	0.04
31	0.07	0.09	0.07
32	0.00	0.01	0.01
33	0.34	0.18	0.94
34	0.46	1.16	2.04
35	0.02	0.21	0.05
37	0.01	0.03	0.01
62	0.03	0.08	0.13
43	0.01	0.03	0.07
44	0.17	0.12	0.65
45	0.02	0.05	0.03
46	0.32	0.26	0.55
47	0.10	0.08	0.23
49	0.10	0.03	0.28

Table 5.2-2 NONDIMENSIONAL CONCENTRATION COEFFICIENTS ($\times 10^5$)
FOR UNIT 16 - SITE 2
AND A WIND DIRECTION OF 230°

	Wind Speed (ms^{-1})		
Location Number	3.2	6.5	9.8
2	0.04	0.09	0.04
4	0.05	0.20	5.52
9	0.01	0.00	0.03
10	0.02	0.05	0.00
11	0.01	2.27	0.86
12	0.03	5.96	4.37
13	0.04	10.25	16.52
14	0.07	3.87	37.27
15	0.05	0.24	6.23
20	0.01	0.04	0.11
21	0.01	0.03	0.08
22	0.01	0.34	0.15
23	0.01	0.03	3.15
24	0.01	0.03	5.29
25	0.08	0.69	13.35
26	0.07	0.25	14.70
27	0.05	0.06	0.37
32	0.01	0.01	0.34
33	0.02	0.06	0.37
34	0.02	0.03	0.46
35	0.00	--	0.67
36	0.02	0.00	0.32
37	0.02	0.02	0.35
38	0.07	0.12	0.61
39	0.04	0.02	0.60
43	0.03	0.04	0.03
44	0.01	0.03	0.08
45	0.02	0.00	0.08
46	0.02	0.06	0.11
47	0.02	0.06	6.47
48	0.00	0.02	0.19
49	0.01	0.03	8.82
50	0.05	0.00	4.70
51	0.00	0.09	4.55

Table 5.2-3 NONDIMENSIONAL CONCENTRATION COEFFICIENTS (x 10^5)
FOR UNIT 16 - SITE 2
AND A WIND DIRECTION OF 250°

	Wind Speed (ms^{-1})		
Location Number	3.2	6.5	9.8
2	0.05	0.00	0.34
4	0.82	2.67	2.44
5	0.13	12.68	61.45
6	0.09	0.09	0.95
11	0.07	0.06	0.62
13	0.13	0.00	0.17
14	0.19	0.09	0.28
15	0.44	1.55	0.95
16	0.07	0.07	0.03
17	0.06	0.00	0.14
18	0.06	0.07	0.00
23	0.10	0.04	0.11
24	0.16	0.03	0.06
25	0.01	0.02	0.08
26	0.15	0.06	0.08
27	0.00	0.06	0.17
28	0.16	0.05	0.14
29	0.03	1.36	11.26
30	0.16	0.09	1.85
35	0.03	0.02	0.25
37	0.16	0.02	0.34
38	0.10	0.06	0.03
39	0.23	1.21	2.19
40	0.05	3.46	5.46
41	0.07	0.77	0.90
42	0.16	0.02	0.11
47	0.14	0.00	0.14
49	0.05	0.09	0.17
50	0.16	0.06	0.20
51	0.05	0.00	0.06
52	0.16	0.06	0.06
53	0.06	1.44	2.24
54	0.12	0.17	0.14

Table 6-1 The Wind Velocity (m/s) at Sites 1 and 6 for Three Heights Above Ground Level for the 9.8 m/s Case*

Prototype Height (m,AGL)	Site 1		Site 6	
	Model m/s	Prototype m/s	Model m/s	Prototype m/s
10 m	0.57	9.3	0.73	11.95
20 m	0.63	10.2	0.86	14.00
40 m	0.70	11.4	0.92	15.20

*The Site 6 windspeed at 10 m should equal 9.8 m/s. However, the free stream velocity was set slightly higher during these hot-wire velocity measurements.